The Meteoritical Society

Meteoritics & Planetary Science 47, Nr 1, 72–98 (2012)
doi: 10.1111/j.1945-5100.2011.01314.x

Compositional constraints on the genesis of diogenites

David W. MITTLEFEHLDT[1*], Andrew W. BECK[2,3], Cin-Ty A. LEE[4], Harry Y. McSWEEN Jr.[2], and Paul C. BUCHANAN[5]

[1]Mail Code KR, Astromaterials Research Office, NASA Johnson Space Center, Houston, Texas 77058, USA
[2]Department of Earth and Planetary Sciences and Planetary Geoscience Institute, University of Tennessee, Knoxville, Tennessee 37996–1410, USA
[3]Present address: Department of Mineral Sciences, Smithsonian Institution, National Museum of Natural History, 10th and Constitution NW, Washington, D.C. 20560–0112, USA
[4]Department of Earth Science, Rice University, Houston, Texas 77005, USA
[5]Kilgore College, 1100 Broadway Blvd., Kilgore, Texas 75662, USA
[*]Corresponding author. E-mail: david.w.mittlefehldt@nasa.gov

(Received 01 June 2011; revision accepted 28 October 2011)

Abstract–We have done bulk rock compositional analyses (INAA, ICP-MS) and petrologic study of a suite of diogenite meteorites. Most contain orthopyroxenes with mg#s of 70.6–79.0. Meteorite Hills (MET) 00425 is magnesian (mg# of 83.9). Lewis Cliff (LEW) 88011 contains orthopyroxene grains of varying mg# (76.3–68.6). Queen Alexandra Range (QUE) 93009 (orthopyroxene mg# 70.6) contains coarse-grained noritic clasts (plagioclase $An_{84.7–88.3}$), and is rich in incompatible trace elements. It has Eu/Eu* < 1, indicating that cumulate norites do not dominate its trace element inventory. Queen Alexandra Range 93009 may be transitional between diogenites and magnesian cumulate eucrites. Lewis Cliff 88679, a dimict breccia of harzburgite and orthopyroxenite, has anomalously low concentrations of highly incompatible elements (e.g., Nb, La, Ta, U) compared to other diogenites, but is similar to them in less highly incompatible elements (e.g., Y, Zr, Yb, Hf). It is unlikely that this characteristic reflects a low proportion of a trapped melt component. The highly incompatible elements were likely mobilized after impact mixing of the two parent lithologies. Graves Nunataks 98108 shows an extreme range in Eu/Eu* attributable to the heterogeneous distribution of plagioclase; one sample has the lowest Eu/Eu* among diogenites. We find no compelling evidence to support the hypothesis that diogenite parent magmas were contaminated by partial melts of the eucritic crust. We posit that subsolidus equilibration between orthopyroxene and minor/trace phases (including phosphates) resulted in preferential redistribution of Eu^{2+} relative to Eu^{3+} and other rare earth elements, and results in anomalously low Eu/Eu* in samples leached in acids that dissolve phosphates.

INTRODUCTION

Asteroid 4 Vesta has been called "the smallest terrestrial planet" because it is the only large asteroid with a basaltic surface (Keil 2002). Identification of the basaltic nature of Vesta's surface was accomplished through reflectance spectroscopy in the visible and near infrared wavelength region utilizing ground-based telescopes, and comparison to laboratory spectra of basaltic achondrites (McCord et al. 1970). McCord et al. (1970) found that the reflectance spectrum of Vesta is a very close match to that of the basaltic eucrite Nuevo Laredo; this led to the hypothesis that Vesta was the parent asteroid of the howardite, eucrite, and diogenite (HED) clan of meteorites (Consolmagno and Drake 1977; Consolmagno 1979; Drake 1979). This hypothesis garnered widespread support when it was shown that there are numerous, < 10 km sized basaltic asteroids distributed in space from near Vesta out to the 3:1 Kirkwood Gap and the ν6 resonance from which gravitational perturbations can send meteoroids into Earth-intersecting orbits (Binzel and Xu 1993).

The study of basaltic eucrites has yielded a consensus view that the eucrite parent asteroid was substantially molten early in its history, and subsequently crystallized. Basaltic eucrites are thought to be quenched residual melts formed during the waning stages of igneous differentiation (see, e.g., Righter and Drake 1997; Ruzicka et al. 1997; Warren 1997; Greenwood et al. 2005). Modeling of the differentiation process to try to match basaltic eucrite major and trace lithophile element and siderophile element contents has resulted in conflicting claims of success (e.g., Righter and Drake 1997; Ruzicka et al. 1997). Nevertheless, it is clear that within the uncertainties of the modeling process, basaltic eucrite compositions can be successfully described as being those of residual melts.

The main competing hypothesis for differentiation of the eucrite parent asteroid is that partial melting produced a series of primary melts from primitive, chondritic source regions of the proto-vestan interior (Stolper 1977). This hypothesis has lost favor for a variety of reasons, including arguments based on major element mass balance (Warren 1985, 1997), the difficulty of explaining the very low siderophile element contents of eucrites (see McSween et al. 2011), and the homogeneity in oxygen isotopic compositions of HEDs (Greenwood et al. 2005).

Although a eucrite-centric view of the differentiation of Vesta permits fairly simple models, diogenites are difficult to fit into such models. Diogenites are a suit of cumulate orthopyroxenites, harzburgites, and a dunite (e.g., Fukuoka et al. 1977; Fowler et al. 1994, 1995; Mittlefehldt 1994, 2000; Shearer et al. 1997, 2010; Barrat et al. 2008, 2010; Beck and McSween 2010; Beck et al. 2011). Mittlefehldt (1994) noted that the range in diogenite minor and trace element concentrations suggested that the suite would represent cumulates from a fairly extensive range in crystallization, and that this was difficult to understand for rocks that are virtually monomineralic orthopyroxene or orthopyroxene + olivine. One would expect that plagioclase crystallization would have occurred if the parent was a magnesian mafic magma (Mittlefehldt 1994). This view was echoed by Fowler et al. (1995) and Shearer et al. (1997, 2010) who suggested that the diogenite suite can most simply be understood as representing a set of cumulates derived from a series of parent magmas with differing initial trace element contents.

Recent compositional study of diogenites has led to the hypothesis that many diogenites were formed by remelting of magma ocean cumulates (Barrat 2004; Barrat et al. 2008). Further, extremely low Eu contents relative to Sm and Gd for many diogenites that had been leached in acid to remove phosphates led to the hypothesis that many diogenite parent magmas were contaminated by melts derived by anatexis of the basaltic (eucritic) crust, and thus must be younger than much of the crust of Vesta (Barrat et al. 2010).

We have undertaken petrologic and bulk compositional studies of a large suite of US Antarctic diogenites and the fall Bilanga to test hypotheses for diogenite petrogenesis and to further understand the constraints diogenites impose on the differentiation of 4 Vesta. One set of bulk samples has been analyzed by instrumental neutron activation analysis (INAA) at NASA Johnson Space Center (JSC), and a second set by inductively coupled plasma–mass spectrometry (ICP-MS) at Rice University. Petrographic and mineral composition studies of thin sections and/or grain mounts have been done at NASA JSC and the University of Tennessee. Preliminary results focusing on the bulk rock compositional studies have been presented (Mittlefehldt 2002; Mittlefehldt et al. 2009). Beck and McSween (2010) presented the petrologic study of several of the diogenites including those analyzed by ICP-MS, and Beck et al. (2011) presented the petrologic and bulk compositional study of the dunitic diogenite Miller Range (MIL) 03443. Here, we present our compositional studies of diogenites, plus the petrologic studies done at NASA JSC.

SAMPLES AND ANALYTICAL METHODS

We obtained 27 samples of 20 Antarctic diogenites from the NASA JSC Astromaterials Curation Office through the Meteorite Working Group, and one sample of the fall Bilanga from the University of Arizona. Table 1 gives details of the samples studied.

Sample Preparation

The samples received were of various masses (Table 1). For the samples requested for INAA, when the sample mass and character allowed, individual coarse-grained clasts or collections of millimeter-sized pyroxene grain separates were prepared for analysis. Brief sample descriptions for these clasts are given in Table 1. For other diogenites, only whole-rock samples were prepared. These were coarsely crushed, homogenized, coned-and-quartered, and representative splits taken for analysis. For some of these samples, small chips were taken to prepare grain mounts for electron microprobe analysis (EMPA). The samples requested for ICP-MS were ground to a fine powder, homogenized, and coned-and-quartered to obtain representative splits for analysis. A few samples had a small amount of exterior material on them, which was removed prior to crushing.

Electron Microprobe Analysis

Grain mounts and/or thin sections were studied for all meteorites. Beck and McSween (2010) presented their EMPA work on thin sections for some of the samples

Table 1. Details of samples studied. The presence, absence, or modal olivine content is given.

Meteorite	Split	Mass received (mg)	Type	Remarks
ALHA77256	,158	483	wr	Olivine diogenite (1); harzburgitic diogenite (2); 10.6% olivine (2)
ALH 85015	,7	383	wr	Polymict diogenite (2) and this study; 4.6% olivine (2)
Bilanga	UA1911,3f,3	644	wr	Fall; no olivine found (3)
EET 83246	,26	485	wr	Dimict diogenite (4); 1.3% olivine (2)
EET 83247	,20	40	opx	Coarse orthopyroxene–chromite grains hand-picked; meteorite contains 0.2% olivine (5)
EET 83247	,21	18	opx	Coarse orthopyroxene grains hand-picked
GRA 98108	,11	243	wr	Harzburgitic diogenite (2); 18.5% olivine (2)
GRA 98108	,22	540	wr	
GRO 95555	,10	527	wr	Unbrecciated, metamorphic (6); no olivine found (6)
GRO 95555	,17	640	wr	
LAP 03979	,6	390	wr	Dimict diogenite (4); 4.6% olivine (2)
LAP 91900	,9	680	opx	Two individual large orthopyroxene grains hand-picked; no olivine found in meteorite (5)
LAP 91900	,10	560	wr	
LAP 91900	,29	420	wr	
LEW 88008	,18	607	wr	Dimict, genomict diogenite (4); 1.6% olivine (2)
LEW 88679	,6	120	brec	Dimict, genomict diogenite (4); 14.6% olivine (2)
LEW 88679	,6	–	opx	Several coarse, green orthopyroxene grains hand-picked
LEW 88679	,10	395	wr	
MET 00422	,6	1074	wr	Basaltic clasts present (initial description)
MET 00424	,10	1150	wr	Olivine present (initial description)
MET 00425	,6	1253	wr	
MET 00436	,9	1080	wr	
MET 00436	,13	840	wr	
MET 001060	,4	525	wr	
MET 01084	,8	368	wr	Dimict, genomict diogenite (4); 6.1% olivine (2)
MIL 03368	,10	613	wr	2.2% olivine (2)
PCA 91077	,4	311	wr	No olivine found (5)
PCA 02008	,6	540	wr	Paired with PCA 02009 howardite (7); polymict diogenite (2) and this study; 3.7% olivine (2)
QUE 93009	,8	270	clast	Several coarse orthopyroxene grains hand-picked; light gray (plagioclase?) material included in some
QUE 93009	,8	–	wr	

Note: References: 1. Sack et al. (1991); 2. Beck and McSween (2010); 3. Domanik et al. (2004); 4. Beck et al. (Forthcoming); 5. Bowman et al. (1997); 6. Papike et al. (2000); 7. Welten et al. (2009).

analyzed here. Mineral analyses reported here were done at JSC using a Cameca SX100 electron microprobe. Pyroxene, olivine, chromite, and ilmenite were analyzed using 20 kV, 40 nA focused electron beam to enhance excitation of the minor transition elements. Plagioclase analyses were performed using a 15 kV, 20 nA focused electron beam, conditions which do not result in measurable mobilization of Na_2O or K_2O from the calcic plagioclases typical of HEDs. However, for Lewis Cliff (LEW) 88011, plagioclase analyses for the more sodic grains showed departures from stoichiometry consistent with loss of Na_2O and K_2O. These analyses were repeated using a 15 kV, 20 nA electron beam rastered over a 10×10 μm area. These conditions allow analysis of the albitic plagioclases of chondrites without loss of Na_2O or K_2O (see Mittlefehldt and Lindstrom 2001). The JSC EMPA standard minerals collection provided the standardization base for the analyses. The Cameca PAP data reduction software was used to calculate mineral compositions.

Instrumental Neutron Activation Analysis

Samples massing between 15 and 180 mg were encapsulated in ultrapure Heraeus Amersil T21 Suprasil®[1] silica glass tubes for neutron irradiation. Six separate INAA irradiations were performed at the

[1]Use of trademarked products does not imply endorsement of the product.

University of Missouri Research Reactor Facility. The irradiation conditions differed slightly from experiment to experiment, with total thermal neutron fluence varying between 2.8×10^{18} and 4.0×10^{18} n cm^{-2}. For each irradiation, four count sets were performed over a period of about 3 months from the time of irradiation to obtain data on nuclides of differing half-lives. Standards used were NIST NBS 1633a (coal flyash) for K, Sc, Se, Br, Sr, Zr, La, Ce, Sm, Eu, Tb, Yb, Lu, Hf, Ta, and Th; GIT-IWG AN-G (Fiskenaesset anorthosite) for Na and Ca; SABS-MINTEK SARM-7 (Merensky Reef precious-metal ore) for Cr, Fe, Co, Ni, and Ir. Raw spectral data were reduced using an updated version of the TEABAGS program of Lindstrom and Korotev (1982). Interference corrections, element concentrations, and final data evaluation were carried out using additional in-house programs. All data were rigorously scrutinized for unanticipated interferences, improperly chosen backgrounds or other problems, and corrections were made as necessary. USGS standard BHVO-1 (Hawaiian basalt) was analyzed in each experiment as a control sample.

Some Na is produced via the ^{24}Mg (n,p) ^{24}Na reaction. This was corrected using the procedure described in Mittlefehldt (1994). Several analyses of empty silica tubes show that the pure silica tubes used to encapsulate samples contain 0.32 ng g^{-1} of La. A blank correction was made for La as described in Mittlefehldt (1994). For some samples, the irradiated rock was transferred to an unirradiated vial prior to counting and blank corrections were unnecessary.

ICP-MS Analysis

Two separate ICP-MS analysis sequences were done, one each in 2008 and 2009. Sample powders used for solution ICP-MS analysis ranged from 49 to 69 mg in mass. Similar sized powders of the standards USGS AGV-1 (Guano Valley andesite), BCR-2 (Columbia River basalt), BIR-1 (Iceland basalt), BHVO-1, DTS-1 (Twin Sisters dunite), PCC-1 (California peridotite), GIT-IWG AN-G, and GSJ JP-1 (Horoman peridotite [dunite]) were also prepared. Sample and standard powders were put into Savillex®[1] beakers, 0.25 mL each of concentrated HF and $HClO_4$ acids were added, and placed in a gravity oven set to 135 °C for approximately 12 h. A procedural blank was run in parallel. After removing the beakers from the oven and allowing them to cool, they were placed on an approximately 170 °C hotplate until complete dryness was attained. This entire process (acid digestion, dry-down) was repeated twice more. After the third repetition, approximately 2 mL of 2% HNO_3 were added to each beaker. New 125 mL each polypropylene bottles were weighed and 10–15 mL of 2% HNO_3 followed by approximately 0.28 mL of concentrated In solution (~446 μg g^{-1}) were added. The contents of the Savillex® beakers were transferred to the polypropylene bottles, which were filled to capacity with 2% HNO_3, and 0.025 mL of concentrated HCl was added to keep Fe in solution. The In concentration of the final solution was approximately 1 ng g^{-1}. The following day the sample solutions were transferred to vials and analyzed using a ThermoFinnigan Element2 Magnetic Sector ICP-MS at Rice University. Analysis parameters were 13.43 L min^{-1} of Ar cool gas, 0.94 L min^{-1} of Ar sample gas, and 0.97 L min^{-1} of Ar carrier (auxiliary) gas. Forward power was 1370 W and reflected power was 2 W. Elements Li, Be, Sc, Ti, V, Cr, Co, Ni, Cu, Zn, Ga, Rb, Sr, Y, Zr, Nb, Cs, Ba, La, Ce, Pr, Nd, Sm, Eu, Gd, Tb, Dy, Ho, Er, Tm, Yb, Lu, Hf, Ta, Tl, Pb, Th, and U were measured in low mass-resolution mode ($m/\Delta m$ of 300), and Na, Al, P, Ca, Sc, Ti, V, Cr, Mn, Fe, Co, Ni, Cu, Zn, Ge, Zr, and Nb were measured in medium mass-resolution mode ($m/\Delta m$ of 4000). BHVO-1 and BIR-1 were used for quantification. Standard JP-1 was also used for quantification of Al, Ca, Sc, V, Cr, Mn, Fe, Co, Ni, and Cu in the 2009 analysis set. Standard values reported by Eggins et al. (1997) were used for quantification. The count rate on ^{115}In was used to compensate for instrumental drift. Procedural blanks were treated in the same manner as samples and standards, and drift-corrected blank intensities were subtracted from all samples and standards prior to external calibration. Uncertainties for the measurements are < 5%.

Splits of the powders prepared for solution ICP-MS were fused into glass beads for major element analysis using a fused-bead furnace at the University of Tennessee, similar to the method described in Brown (1977). Too little powder of Meteorite Hills (MET) 01084 was left to make a fused bead. We initially planned to measure major element compositions of the glass beads by electron microprobe. However, it was discovered that Fe and Mg distributions in the beads were heterogeneous with depth as exposed by sample preparation (Beck et al. 2008). Because of this, we opted to use a laser ablation ICP-MS (LA-ICP-MS) technique. The laser ablation method "drills down" into the bead and partially mitigates problems associated with surface analyses by EMPA when depth-related heterogeneities are present. The LA-ICP-MS analysis was carried out at Rice University on the same ICP-MS as used for solution analyses, but coupled to a 213 nm laser (New Wave UP-213SS). The Rice University LA-ICP-MS procedures are documented in Lee et al. (2008). Five spots with a size of 44 μm were analyzed on each bead. The beads were ablated with an energy flux of 16–18 J cm^{-2} at a 10 Hz repetition rate. Ablation duration ranged from 30 to 40 s. The ablated material was

transported with He carrier gas and mixed with Ar gas before entering the ICP torch. The concentration of Ca was measured in each bead by EMPA prior to laser ablation and was used as an internal standard. The Ca concentration is homogeneous throughout the bead (Beck et al. 2008). Count rates of ^{23}Na, ^{25}Mg, ^{27}Al, ^{30}Si, ^{49}Ti, ^{52}Cr, ^{55}Mn, and ^{57}Fe were determined in medium mass-resolution mode ($m/\Delta m$ of 4000), which was sufficient to resolve all isobaric interferences. USGS basaltic glasses BHVO-2G, BIR-1G, and BCR-2G were used as external standards for quantification. Three sigma standard deviations (internal precision) were $< 1\%$, except for ^{23}Na where it was 2%.

RESULTS

Mineral Compositions

Beck and McSween (2010) presented their mineral compositional data for all samples analyzed here by ICP-MS. The EMPA work carried out at JSC includes some of these meteorites plus those we have analyzed by INAA. Tables 2–5 present representative mineral compositions from the JSC analyses.

Low-Ca pyroxene compositions (Table 2) are for the most part within the range typical of diogenites, with mg# (molar 100*(MgO/(MgO + FeO)) in the range 70–77. MET 00425 is exceptional with an mg# of 83.8. This is one of the most magnesian diogenites (Mittlefehldt 2002; Barrat et al. 2008) with an average orthopyroxene mg# greater than those of Bilanga (79.8; Domanik et al. 2004), the magnesian fraction of Elephant Moraine (EETA or EET) 79002 (80.4; Mittlefehldt 2000), or the magnesian fraction of LaPaz Icefield (LAP) 02216 (78.9; Beck and McSween 2010). Only Northwest Africa (NWA) 1461 with an mg# of approximately 86 (Bunch et al. 2007; Barrat et al. 2010) is more magnesian than MET 00425. LEW 88011 contains the most ferroan orthopyroxenes we analyzed, with mg#s as low as 68.6. However, this diogenite contains pyroxenes with a range of compositions, the most magnesian of which has an mg# of 76.3, within the range typical of diogenites (e.g., Mittlefehldt 1994). Pyroxenes in LEW 88011 are unzoned, but some low-Ca pyroxenes contain augite exsolution lamellae and some augite grains contain low-Ca pyroxene exsolution lamellae. Queen Alexandra Range (QUE) 93009 is also ferroan; most pyroxene grains in it have mg#s of 70.1–70.7, but a few are as magnesian as mg# 71.4. Figure 1 is an mg# histogram for average low-Ca pyroxene grains in diogenites from this work and the literature. Some diogenites have two or more distinct populations of pyroxenes (Mittlefehldt 2000; Beck and McSween 2010) and for these, population averages are shown. For LEW 88011, which shows an unusually wide range in pyroxene mg#, individual grain compositions are shown.

Pecora Escarpment (PCA) 02017 contains a variety of pyroxenes from typical diogenite orthopyroxenes to ferroan eucritic low-Ca pyroxenes (Table 2). Diogenitic orthopyroxenes have mg#s of 77.5–74.2 and $Wo_{2.0–2.5}$. Some of the ferroan low-Ca pyroxenes have mg#s of approximately 64–54 and $Wo_{2.8–3.6}$; one has a composition of $Wo_{11.5}En_{48.9}Fs_{39.5}$. These are similar to cumulate eucrite pyroxenes (cf. Mittlefehldt et al. 1998). Other ferroan pyroxenes are similar to basaltic eucrite pyroxenes (mg#s 40–35, $Wo_{21–27}$). One pyroxene grain is more ferroan than those of the evolved eucrites Lakangaon and Nuevo Laredo—mg# 27.7 versus 32–33 (Mason et al. 1979).

Oxide compositions are given in Table 3. Chromite is found in all diogenites, whereas ilmenite is present in only QUE 93009 among the diogenites we have analyzed. As noted by Bowman et al. (1999) and Mittlefehldt (1994), Allan Hills (ALHA or ALH) 77256 contains the most aluminous chromites. The most Al-poor grain in this meteorite has a higher Al content than all but one grain from all other diogenites studied here (Fig. 2). However, some chromite grains in Ellemeet, EET 83246, and LEW 88008 are as aluminous as or more so than those in ALHA77256 (Bowman et al. 1999). ALHA77256 chromites are also the most magnesian; the least magnesian grain has the lowest Al content. Chromite grains in magnesian diogenite MET 00425 are not unusually Mg-rich. They have mg#s within the range of other diogenites, and have Al contents at the low end of the range (Fig. 2). Chromite grains in ferroan diogenite QUE 93009 are the most ferroan studied here. They are comparable to chromite grains in Yamato (Y) Type B (Y-75032 type) diogenites in mg# and Al content (Mittlefehldt and Lindstrom 1993). Ilmenite is rarely reported as a discrete phase from diogenites but is present in Yamato Type B diogenites (Mittlefehldt and Lindstrom 1993). Ilmenite as exsolution lamellae are present in the chromite grains in QUE 93009, but discrete ilmenite grains were not found.

Only a few of the diogenites investigated here contain olivine; representative data are presented in Table 4. Our analyses agree with those of Beck and McSween (2010). We analyzed four olivine grains in PCA 02017. This diogenite is paired with PCA 02008, which was studied by Beck and McSween (2010). Olivines in PCA 02017 are similar in composition to those in PCA 02008 except that they have higher CaO contents, 0.13–0.17 wt% versus 0.07 ± 0.03 (Beck and McSween 2010).

Several of the diogenites we have studied contain plagioclase; representative analyses are given in Table 5.

Table 2. Representative pyroxene compositions of diogenites determined by electron microprobe analysis.

Meteorite	ALHA 77256	ALHA 77256	GRA 98108	GRA 98108	GRO 95555	LAP 91900	LEW 88011	LEW 88011	LEW 88011	LEW 88011	LEW 88011	LEW 88011
Specific	,154	,155	,16	,16	,21	,9	,4	,4	,4	,4	,4	,4
SiO_2	54.2	52.4	54.6	52.8	54.4	54.2	54.5	53.9	53.7	53.2	52.9	53.4
TiO_2	0.11	0.28	0.16	0.26	0.06	0.06	0.10	0.13	0.22	0.23	0.41	0.35
Al_2O_3	0.79	1.62	0.86	1.34	0.57	0.59	0.92	1.03	1.01	0.94	1.12	1.09
Cr_2O_3	0.85	0.74	0.38	0.69	0.80	0.65	0.84	0.76	0.75	0.56	0.87	0.39
FeO	15.2	5.6	14.3	5.4	15.4	15.7	15.1	16.2	16.9	19.1	7.3	6.1
MnO	0.533	0.279	0.511	0.274	0.501	0.557	0.469	0.502	0.554	0.638	0.325	0.270
MgO	27.3	16.2	27.0	16.2	26.9	27.0	27.2	26.2	25.3	23.4	15.6	16.2
CaO	0.79	22.3	1.82	22.3	1.05	1.13	1.17	1.33	1.93	2.04	21.5	22.3
Sum	99.773	99.419	99.631	99.264	99.681	99.887	100.299	100.052	100.364	100.108	100.025	100.100
Molar quantities												
Fe/Mn	28.1	20.0	27.6	19.6	30.3	27.9	31.7	31.8	30.1	29.5	22.3	22.2
Fe/Mg	0.312	0.196	0.296	0.188	0.322	0.327	0.311	0.346	0.374	0.457	0.264	0.211
mg#	76.2	83.6	77.2	84.2	75.7	75.4	76.3	74.3	72.8	68.6	79.1	82.6
Wo %	1.57	45.4	3.60	45.4	2.08	2.22	2.30	2.63	3.84	4.11	44.0	45.0
En %	75.0	45.7	74.4	45.9	74.1	73.7	74.5	72.3	70.0	65.8	44.3	45.4
Fs %	23.4	8.95	22.0	8.63	23.8	24.1	23.2	25.0	26.2	30.1	11.7	9.57
Atoms per six oxygens												
Si	1.9638	1.9414	1.9726	1.9545	1.9747	1.9668	1.9636	1.9582	1.9548	1.9625	1.9579	1.9649
Ti	0.0031	0.0078	0.0042	0.0073	0.0017	0.0015	0.0028	0.0036	0.0061	0.0063	0.0115	0.0096
Al	0.0339	0.0706	0.0367	0.0586	0.0242	0.0251	0.0392	0.0439	0.0431	0.0408	0.0491	0.0471
Cr	0.0244	0.0216	0.0110	0.0203	0.0229	0.0186	0.0240	0.0217	0.0215	0.0164	0.0255	0.0114
Fe	0.4591	0.1749	0.4314	0.1682	0.4672	0.4774	0.4537	0.4914	0.5143	0.5887	0.2272	0.1869
Mn	0.0164	0.0088	0.0157	0.0086	0.0154	0.0171	0.0143	0.0154	0.0171	0.0199	0.0102	0.0084
Mg	1.4726	0.8933	1.4571	0.8952	1.4530	1.4593	1.4592	1.4196	1.3738	1.2874	0.8598	0.8875
Ca	0.0308	0.8864	0.0706	0.8858	0.0409	0.0440	0.0451	0.0516	0.0754	0.0805	0.8522	0.8788

Meteorite	LEW 88679	LEW 88679	MET 001060	MET 00422	MET 00424	MET 00425	MET 00436	MET 00855	MET 01084	MET 01084
Specific	,6	,5	,7	,9	,14	,10	,15	,6	,6	,6
SiO_2	54.1	54.1	55.7	54.1	53.9	56.0	54.0	54.7	54.9	54.1
TiO_2	0.19	0.18	0.06	0.04	0.02	0.03	0.02	0.03	0.18	0.25
Al_2O_3	1.23	1.14	0.44	0.49	0.27	0.42	0.25	0.30	0.94	0.62
Cr_2O_3	0.42	0.61	0.31	0.59	0.30	0.70	0.17	0.20	0.63	0.34
FeO	15.7	17.2	13.7	16.7	18.3	10.7	18.3	18.6	14.6	18.4
MnO	0.549	0.609	0.592	0.578	0.696	0.364	0.677	0.722	0.496	0.653
MgO	26.7	24.8	29.1	26.4	25.5	31.2	25.6	25.3	27.8	25.0
CaO	1.68	2.04	0.64	0.94	0.75	0.50	0.79	0.82	1.16	1.24
Sum	100.569	100.679	100.542	99.838	99.736	99.914	99.807	100.672	100.706	100.603
Molar quantities										
Fe/Mn	28.2	27.9	22.9	28.5	26.0	29.0	26.7	25.5	29.1	27.9
Fe/Mg	0.330	0.390	0.264	0.354	0.404	0.193	0.402	0.413	0.296	0.414

Table 2. *Continued.* Representative pyroxene compositions of diogenites determined by electron microprobe analysis.

Meteorite	LEW 88679	LEW 88679	MET 001060	MET 00422	MET 00424	MET 00425	MET 00436	MET 00855	MET 01084	MET 01084
Specific	,6	,5	,7	,9	,14	,10	,15	,6	,6	,6
mg#	75.2	71.9	79.1	73.9	71.3	83.9	71.3	70.8	77.2	70.7
Wo %	3.30	4.09	1.23	1.85	1.49	0.95	1.55	1.62	2.27	2.46
En %	72.7	69.0	78.1	72.5	70.2	83.1	70.2	69.6	75.4	69.0
Fs %	24.0	26.9	20.7	25.7	28.3	16.0	28.2	28.8	22.3	28.6
Atoms per six oxygens										
Si	1.9529	1.9648	1.9807	1.9717	1.9794	1.9776	1.9815	1.9882	1.9641	1.9720
Ti	0.0052	0.0049	0.0016	0.0012	0.0005	0.0007	0.0006	0.0008	0.0048	0.0068
Al	0.0523	0.0488	0.0183	0.0209	0.0119	0.0175	0.0108	0.0130	0.0394	0.0264
Cr	0.0121	0.0176	0.0087	0.0169	0.0088	0.0195	0.0048	0.0057	0.0178	0.0098
Fe	0.4726	0.5227	0.4082	0.5077	0.5629	0.3161	0.5623	0.5670	0.4373	0.5620
Mn	0.0168	0.0187	0.0178	0.0178	0.0217	0.0109	0.0211	0.0222	0.0150	0.0201
Mg	1.4328	1.3403	1.5447	1.4354	1.3951	1.6419	1.3981	1.3727	1.4798	1.3574
Ca	0.0650	0.0794	0.0243	0.0365	0.0295	0.0189	0.0309	0.0319	0.0445	0.0485

Meteorite	PCA 02017	PCA 02017	PCA 02017	PCA 02017	PCA 02017	PCA 02017	PCA 02017	PCA 02017	PCA 02017	QUE 93009	QUE 93009
Specific	,4	,4	,4[a]	,4[a]	,4[a]	,4[a]	,4[a]	,4[a]	,4	,9	,9
SiO_2	55.2	54.2	51.4	53.1	51.3	49.3	48.1	48.7	52.5	52.9	54.1
TiO_2	0.10	0.09	0.34	0.01	0.51	0.49	0.69	0.80	0.00	0.30	0.21
Al_2O_3	0.79	0.73	0.68	0.57	1.07	1.05	0.96	1.29	0.82	0.98	0.38
Cr_2O_3	0.76	0.65	0.26	0.38	0.60	0.41	0.36	0.30	0.50	0.36	0.34
FeO	14.5	16.4	27.1	22.1	24.4	27.9	32.3	27.6	10.9	18.1	6.2
MnO	0.500	0.584	0.900	0.964	0.815	0.908	1.006	1.061	0.576	0.602	0.269
MgO	27.9	26.5	18.1	21.6	17.0	10.2	6.9	8.2	15.1	24.5	16.7
CaO	1.02	1.29	1.35	1.77	5.57	9.63	9.76	12.0	19.6	1.94	22.0
Sum	100.770	100.444	100.130	100.494	101.265	99.888	100.076	99.951	99.996	99.682	100.199
Molar quantities											
Fe/Mn	28.6	27.8	29.7	22.6	29.6	30.3	31.7	25.7	18.7	29.6	22.8
Fe/Mg	0.291	0.347	0.842	0.574	0.808	1.533	2.614	1.886	0.406	0.414	0.209
mg#	77.5	74.2	54.3	63.5	55.3	39.5	27.7	34.7	71.1	70.7	82.7
Wo %	1.99	2.53	2.84	3.60	11.5	21.1	21.9	26.6	39.9	3.86	43.9
En %	75.90	72.3	52.7	61.2	48.9	31.1	21.6	25.4	42.7	68.0	46.4
Fs %	22.10	25.1	44.4	35.2	39.5	47.7	56.5	48.0	17.3	28.1	9.69
Atoms per 6 oxygens											
Si	1.9693	1.9617	1.9690	1.9784	1.9434	1.9549	1.9494	1.9433	1.9670	1.9518	1.9858
Ti	0.0027	0.0025	0.0097	0.0002	0.0145	0.0147	0.0209	0.0239	0.0001	0.0083	0.0059
Al	0.0334	0.0313	0.0308	0.0249	0.0478	0.0491	0.0460	0.0605	0.0364	0.0425	0.0165
Cr	0.0214	0.0187	0.0078	0.0112	0.0180	0.0130	0.0114	0.0096	0.0147	0.0105	0.0099
Fe	0.4330	0.4973	0.8686	0.6884	0.7744	0.9246	1.0957	0.9229	0.3417	0.5574	0.1908
Mn	0.0151	0.0179	0.0292	0.0304	0.0262	0.0305	0.0345	0.0359	0.0183	0.0188	0.0084
Mg	1.4869	1.4315	1.0312	1.1993	0.9589	0.6030	0.4192	0.4895	0.8419	1.3475	0.9127
Ca	0.0389	0.0500	0.0556	0.0705	0.2262	0.4095	0.4238	0.5123	0.7871	0.0766	0.8650

[a]Pyroxenes from mafic clasts.

Table 3. Representative chromite and ilmenite compositions determined by electron microprobe analysis.

Meteorite	ALHA 77256	ALHA 77256	GRA 98108	GRA 98108	GRO 95555	LEW 88011	LEW 88011	LEW 88679	LEW 88679	MET 00422	MET 00422
Specific	,155	,155	,16	,16	,21	,4	,4	,5	,5	,9	,9
TiO_2	0.75	0.75	1.13	1.23	0.69	2.20	1.35	1.27	0.86	0.44	0.38
SiO_2	0.00	0.01	0.00	0.02	0.00	0.02	0.05	0.01	0.04	0.00	0.00
Cr_2O_3	46.1	46.1	52.5	47.9	56.9	52.5	50.5	46.5	47.9	60.4	59.2
Al_2O_3	21.4	21.2	15.1	16.2	9.0	10.3	13.4	17.5	15.7	8.86	8.89
V_2O_3[a]	0.25	0.25	0.38	0.74	0.57	0.50	0.45	0.46	0.48	0.40	0.39
FeO[b]	26.2	25.5	25.9	29.3	27.7	31.1	30.5	30.6	30.9	28.7	29.7
MnO	0.410	0.410	0.447	0.570	0.711	0.468	0.456	0.570	0.594	0.482	0.500
MgO	6.10	6.67	5.76	4.81	4.58	2.88	3.21	4.05	3.68	2.69	2.12
CaO	0.02	0.05	0.02	0.06	0.01	0.01	0.01	0.02	0.08	0.00	0.01
Sum	101.230	100.940	101.237	100.830	100.161	99.978	99.926	100.980	100.234	101.972	101.190
Molar quantities											
Fe/Mn	63.1	61.3	57.1	50.8	38.5	65.6	65.9	52.9	51.4	58.9	58.7
mg#	29.3	31.8	28.4	22.6	22.7	14.2	15.8	19.1	17.5	14.3	11.3
cr#	59.0	59.3	70.0	66.5	80.9	77.4	71.7	64.0	67.2	82.0	81.7
Atoms per four oxygens (*chromite*) *or three oxygens* (*ilmenite*)											
Ti	0.0180	0.0181	0.0279	0.0308	0.0179	0.0574	0.0347	0.0317	0.0217	0.0112	0.0099
Si	0.0000	0.0004	0.0000	0.0006	0.0000	0.0006	0.0017	0.0003	0.0012	0.0000	0.0000
Cr	1.1623	1.1642	1.3642	1.2582	1.5551	1.4429	1.3661	1.2179	1.2795	1.6336	1.6226
Al	0.8066	0.7982	0.5839	0.6334	0.3665	0.4213	0.5402	0.6847	0.6245	0.3577	0.3629
V	0.0064	0.0063	0.0099	0.0197	0.0159	0.0138	0.0124	0.0123	0.0130	0.0109	0.0108
Fe^{2+}	0.6992	0.6797	0.7114	0.8143	0.8012	0.9038	0.8717	0.8471	0.8732	0.8232	0.8611
Mn	0.0111	0.0111	0.0125	0.0160	0.0208	0.0138	0.0132	0.0160	0.0170	0.0140	0.0147
Mg	0.2900	0.3173	0.2825	0.2381	0.2357	0.1492	0.1638	0.1999	0.1854	0.1370	0.1094
Ca	0.0008	0.0018	0.0007	0.0020	0.0002	0.0003	0.0004	0.0006	0.0030	0.0000	0.0005

Meteorite	MET 00424	MET 00424	MET 00425	MET 00425	MET 00436	QUE 93009	QUE 93009	QUE 93009	QUE 93009
Specific	,14	,14	,10	,10	,15	,9	,9	,9	,9
TiO_2	0.32	0.17	0.20	0.18	0.41	0.85	1.05	0.52	52.0
SiO_2	0.00	0.00	0.00	0.00	0.00	0.00	0.01	0.03	0.09
Cr_2O_3	64.0	65.6	65.3	63.0	61.9	59.4	54.9	54.7	1.23
Al_2O_3	5.72	3.74	5.70	6.85	7.32	8.66	9.14	9.36	0.07
V_2O_3[a]	0.49	0.41	0.21	0.21	0.50	0.30	0.57	0.54	0.00
FeO[b]	27.7	28.3	24.8	26.5	28.8	29.8	32.4	31.5	43.6
MnO	0.582	0.538	0.456	0.477	0.553	0.499	0.607	0.588	0.979
MgO	3.05	2.31	4.93	3.78	2.44	2.01	1.84	2.01	2.90
CaO	0.01	0.02	0.01	0.02	0.00	0.01	0.03	0.02	0.11
Sum	101.872	101.088	101.606	101.017	101.923	101.529	100.547	99.268	100.979
Molar quantities									
Fe/Mn	46.9	52.0	53.6	54.9	51.4	59.1	52.7	52.9	44.0
mg#	16.4	12.7	26.2	20.2	13.1	10.7	9.20	10.2	10.6
cr#	88.2	92.2	88.5	86.1	85.0	82.2	80.1	79.7	92.6
Atoms per four oxygens (*chromite*) *or three oxygens* (*ilmenite*)									
Ti	0.0082	0.0044	0.0052	0.0046	0.0107	0.0220	0.0278	0.0137	0.9640
Si	0.0000	0.0000	0.0000	0.0000	0.0000	0.0000	0.0004	0.0009	0.0023
Cr	1.7558	1.8404	1.7720	1.7238	1.6911	1.6228	1.5242	1.5340	0.0240
Al	0.2339	0.1561	0.2307	0.2795	0.2983	0.3526	0.3781	0.3916	0.0019
V	0.0137	0.0117	0.0059	0.0059	0.0137	0.0083	0.0159	0.0153	0.0001
Fe^{2+}	0.8033	0.8400	0.7108	0.7677	0.8322	0.8622	0.9512	0.9347	0.8985
Mn	0.0171	0.0162	0.0133	0.0140	0.0162	0.0146	0.0180	0.0177	0.0204
Mg	0.1577	0.1218	0.2524	0.1948	0.1255	0.1035	0.0964	0.1063	0.1066
Ca	0.0003	0.0008	0.0003	0.0006	0.0001	0.0002	0.0009	0.0008	0.0028

[a]Vanadium corrected for Ti K_β interference.
[b]All Fe as FeO.

Table 4. Representative olivine compositions in diogenites determined by electron microprobe analysis.

Meteorite	ALHA 77256	GRA 98108	LEW 88679	PCA 02017
Specific	,155	,16	,5	,4
SiO_2	37.9	38.0	38.1	38.2
TiO_2	< 0.01	0.01	0.02	0.01
Al_2O_3	< 0.01	0.01	0.07	0.02
Cr_2O_3	0.01	0.02	0.02	0.03
FeO	25.1	24.4	25.6	24.2
MnO	0.530	0.529	0.530	0.554
MgO	36.5	36.6	36.3	37.8
CaO	0.055	0.053	0.043	0.13
Sum	100.095	99.622	100.683	100.944
Molar quantities				
Fe/Mn	46.8	45.5	47.6	43.2
Fe/Mg	0.386	0.373	0.396	0.360
mg#	72.1	72.8	71.7	73.5
Atoms per four oxygens				
Si	0.9988	1.0025	1.0006	0.9942
Ti	0.0000	0.0001	0.0004	0.0002
Al	0.0001	0.0004	0.0022	0.0005
Cr	0.0003	0.0005	0.0005	0.0005
Fe	0.5540	0.5384	0.5614	0.5276
Mn	0.0118	0.0118	0.0118	0.0122
Mg	1.4343	1.4417	1.4195	1.4664
Ca	0.0016	0.0015	0.0012	0.0037

For those diogenites investigated by Beck and McSween (2010) and us, plagioclase compositions agree well for LEW 88679 and MET 01084. For Graves Nunataks (GRA) 98108, our plagioclase grains are more sodic ($Ab_{10.5–13.0}$) compared to the representative analysis presented by Beck and McSween (2010), $Ab_{8.6}$. Plagioclase grains in PCA 02017 and QUE 93009 have compositions ($Ab_{6.7–10.0}$ and $Ab_{9.9–16.0}$) that are within the range found for diogenites ($Ab_{4.3–16.1}$; Beck and McSween 2010). The representative plagioclase analysis for PCA 02008 (Beck and McSween 2010) is more sodic than those we have measured in paired meteorite PCA 02017. LEW 88011 is unique. Plagioclase grains in this diogenite are quite variable in composition from $Ab_{10.0–21.4}$, and individual grains can be heterogeneous ($Ab_{17.1–24.6}$ is the extreme case; Table 5). Because of the difficulty in analyzing these plagioclase grains (see above), we did not attempt to determine whether systematic zoning is present. In the grain showing extreme heterogeneity, the randomly selected analysis regions do not show obvious zoning toward grain margins. Plagioclase grains in LEW 88011 show departures from stoichiometry that are correlated with Na content. This is not an artifact of the analyses as our most recent analyses were carried out using conditions that produce stoichiometric analyses of chondritic plagioclase grains as sodic as Ab_{83} (Mittlefehldt and Lindstrom 2001).

Bulk Compositions

Concentrations of major and minor elements determined by LA-ICP-MS on fused beads are given in Table 6. The concentrations of MgO, CaO, and FeO fall within ranges found for diogenites (e.g., Fukuoka et al. 1977; Mittlefehldt 1994; Barrat et al. 2008). The two harzburgite samples, ALHA77256 and GRA 98108, are the most Mg-rich of the group. GRA 98108 is very close in MgO concentration to the most magnesian diogenites, MET 00425 and NWA 1461 (Figs. 3a and 3b) (Barrat et al. 2008; Warren et al. 2009). The Mg-rich nature of the harzburgitic samples is attributed to their high content of olivine (Beck and McSween 2010), which has a higher cation/SiO_2 than does orthopyroxene. LEW 88008 has a high FeO concentration, which is consistent with the relatively ferroan orthopyroxene it contains (Mittlefehldt 1994; Beck and McSween 2010). The CaO contents of samples from this study are within the range found for diogenites (Fig. 3a), but four stand out as being richer in CaO compared to most: ALH 85015, LAP 03979, LEW 88008, and PCA 02008. These meteorites contain higher modal plagioclase than other diogenites, 1.3–5.0 vol% versus < 0.4 vol% (Beck and McSween 2010). These four diogenites are also richer in Al_2O_3 compared to most diogenites (Fig. 3b) and have high Na_2O contents (Table 6), characteristics that are consistent with their higher modal plagioclase content. Excluding the four with high modal plagioclase, the diogenites we analyzed show increasing Al_2O_3 with TiO_2, within the ranges determined for diogenites generally (Fig. 3c).

The results of our INAA on 21 samples of 13 diogenites are presented in Table 7, and the analytical uncertainties are given in the Supporting Information Table S1. Our INAA results and uncertainties on standard reference materials run as control samples are compared to recommended values in the Supporting Information Tables S2 and S3. For most diogenites, only whole-rock samples were analyzed. However, for LAP 91900, LEW 88679, and QUE 93009, we analyzed both whole-rock and separated clast samples. For LAP 91900, two orthopyroxene separates are essentially the same in composition as two whole-rock samples. By contrast, the whole-rock sample of QUE 93009 is substantially richer in incompatible elements compared to the separated coarse-grained clast, with the more highly incompatible elements (e.g., Na, K, La) having higher concentrations relative to the clast sample than do the less highly incompatible elements (e.g., Sc, Yb, Lu) (Table 7). The whole-rock sample of LEW 88679 is richer in Na, La, and Eu compared to the clast sample by approximately 80–100%. We analyzed two orthopyroxene separates for EET 83247. A previous whole rock analysis (Mittlefehldt

Table 5. Representative plagioclase compositions determined by electron microprobe analysis.

Meteorite	GRA 98108	LEW 88011	LEW 88011	LEW 88011	LEW 88011	LEW 88011	LEW 88011	LEW 88679	MET 01084	PCA 02017	PCA 02017	QUE 93009	QUE 93009	QUE 93009
Specific	,15	,4[a]	,4[a]	,4[a]	,4	,4	,4	,5	,6	,4	,4	,9	,9	,9
SiO_2	46.1	50.1	48.4	51.4	46.8	46.3	48.8	44.9	44.5	44.8	46.0	46.0	45.6	47.1
Al_2O_3	34.6	32.4	33.4	31.8	34.3	34.7	33.1	35.6	35.2	35.1	34.6	34.6	35.0	34.0
FeO	0.08	0.17	0.13	0.13	0.15	0.18	0.30	0.13	0.13	0.54	0.31	0.03	0.19	0.10
MgO	< 0.01	0.07	0.05	0.07	0.05	0.04	0.09	< 0.01	0.02	0.02	0.01	< 0.01	< 0.01	< 0.01
CaO	17.7	15.5	16.6	14.8	17.3	17.8	16.1	18.6	18.7	18.5	18.2	17.8	18.2	17.0
Na_2O	1.37	2.35	1.90	2.71	1.43	1.19	1.87	0.861	0.810	0.823	1.12	1.34	1.10	1.76
K_2O	0.088	0.15	0.068	0.20	0.066	0.045	0.11	0.010	0.031	0.044	0.064	0.037	0.033	0.062
Sum	99.938	100.740	100.548	101.110	100.096	100.255	100.370	100.101	99.391	99.827	100.304	99.807	100.123	100.022
Molar quantities														
An	87.3	77.7	82.5	74.2	86.7	89.0	82.1	92.2	92.6	92.3	89.7	87.9	89.9	83.9
Ab	12.2	21.4	17.1	24.6	12.9	10.7	17.2	7.72	7.27	7.41	9.98	11.9	9.88	15.7
Or	0.52	0.90	0.40	1.20	0.39	0.27	0.65	0.06	0.18	0.26	0.38	0.22	0.19	0.36
Atoms per eight oxygens														
Si	2.1212	2.2696	2.2054	2.3121	2.1453	2.1229	2.2232	2.0677	2.0667	2.0741	2.1141	2.1198	2.0982	2.1621
Al	1.8783	1.7274	1.7902	1.6862	1.8549	1.8762	1.7755	1.9340	1.9295	1.9143	1.8747	1.8785	1.9003	1.8373
Fe	0.0032	0.0063	0.0051	0.0048	0.0057	0.0069	0.0114	0.0049	0.0052	0.0209	0.0118	0.0012	0.0075	0.0039
Mg	0.0002	0.0047	0.0037	0.0044	0.0037	0.0024	0.0058	0.0000	0.0013	0.0015	0.0005	0.0000	0.0000	0.0001
Ca	0.8729	0.7510	0.8095	0.7133	0.8521	0.8765	0.7874	0.9201	0.9284	0.9197	0.8956	0.8808	0.8955	0.8358
Na	0.1223	0.2067	0.1674	0.2363	0.1272	0.1054	0.1652	0.0770	0.0730	0.0738	0.0997	0.1192	0.0984	0.1566
K	0.0052	0.0087	0.0040	0.0115	0.0039	0.0026	0.0062	0.0006	0.0018	0.0026	0.0038	0.0022	0.0019	0.0036

[a]Most heterogeneous grain; first column is the average composition, second is most calcic analysis, third is most sodic analysis.

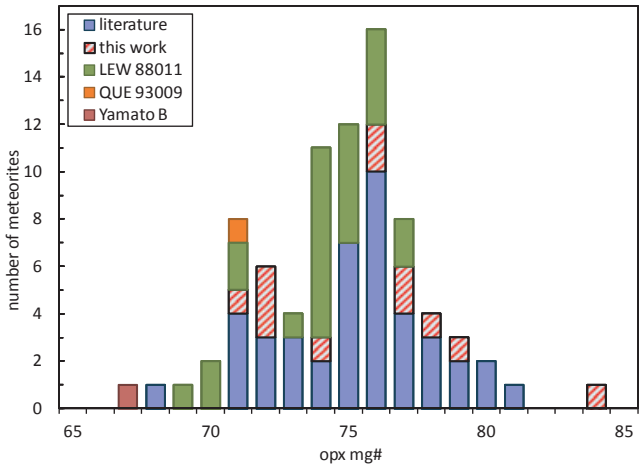

Fig. 1. Histogram of orthopyroxene mg# (100*molar MgO/(MgO + FeO)) for diogenites. Shown are average pyroxene compositions for individual meteorites except for LEW 88011 where grain averages are shown for this heterogeneous diogenite. Literature data are from Beck and McSween (2010), Beck et al. (2011), Domanik et al. (2004), Fowler et al. (1994), Gooley (1972), Mittlefehldt (1994, 2000), and Mittlefehldt and Lindstrom (1993).

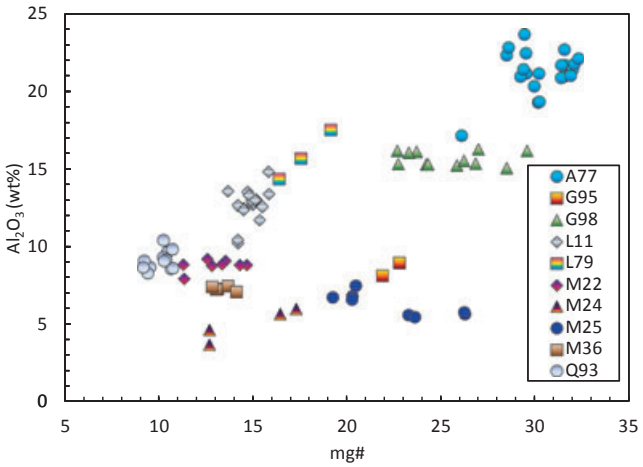

Fig. 2. Al_2O_3 versus mg# for chromite grains analyzed here. A77 = ALHA77256; G95 = Grosvenor Mountains (GRO) 95555; G98 = GRA 98108; L11 = LEW 88011; L79 = LEW 88679; M22 = MET 00422; M24 = MET 00424; M25 = MET 00425; M36 = MET 00436; Q93 = QUE 93009.

1994) is repeated in Table 7. The whole-rock sample of EET 83247 is approximately 2.3–2.5 times richer in Ca, La, Yb, and Lu compared to the orthopyroxene separates, whereas Sc and Na are roughly the same (0.9–1.2 times). Several diogenites are unusually Na-rich. The separated clast from QUE 93009 contains 366 μg g^{-1} Na, compared to a range of 20–120 μg g^{-1} for most orthopyroxene separates (Mittlefehldt 1994, 2000). High Na content in some diogenite samples, including in some orthopyroxene separates, was ascribed to inclusion of plagioclase (Mittlefehldt 1994). This is plausible for QUE 93009 as this meteorite contains abundant plagioclase, and some coarse igneous clasts are noritic (a plagioclase + orthopyroxene rock). One of the two orthopyroxene separates of EET 83247 is also rich in Na (670 μg g^{-1}) and K (360 μg g^{-1}). The Na content would be consistent with inclusion of 4–11% plagioclase in the sample, depending on composition (cf. Table 6). However, the K content is too high to be explained by inclusion of plagioclase of composition similar to those in diogenites, and Eu should have been detected if included plagioclase had a composition similar to those from Johnstown or Dhofar 700 (Mittlefehldt 1979; Barrat et al. 2010). The grain mounts prepared from our allocation did not contain plagioclase, and we have not studied EET 83247 in thin section. Plagioclase has not been found in this diogenite (Bowman et al. 1997).

Table 8 presents our solution ICP-MS analyses on duplicate whole-rock samples of 10 diogenites, and the analytical uncertainties are given in the Supporting Information Table S4. Our ICP-MS results and uncertainties on standard reference materials run as control samples are compared to recommended values in the Supporting Information Table S5. For the most part, our results fall within the ranges previously established for diogenites. Split (c) of ALH 85015 has an Ni content of 979 μg g^{-1}, higher than found for any other diogenite sample, excluding sample E-4 of Ellemeet which was a chondritic clast (Mittlefehldt 1994). Split (a) of ALH 85015 has a much lower Ni content, 130 μg g^{-1}. This difference plausibly reflects the "nugget effect" and a single grain of kamacite approximately 300 μm in size could contribute the additional Ni. For all other samples, our analyses replicate the Ni content to within 30% or less. ALH 85015 and PCA 02008 are richer in the most highly incompatible lithophile elements. The *minimum* concentrations for these two meteorites are greater than the *maximum* concentrations for the other eight diogenites for P, Sr, Nb, Ba, La, Ce, Pr, Nd, Eu, Ta, and Th.

DISCUSSION

We will use our data to evaluate hypotheses for the formation of diogenites. In discussing our data, we will include recent, comparable literature data to widen the range of diogenites under consideration. Before delving into the petrogenesis of diogenites, we will discuss several unusual samples and anomalous data to eliminate noncomparable rocks or nonrepresentative samples from consideration.

EET 83246 and LEW 88008—Altered Diogenites

At the start of meteorite collecting from the stranding surfaces in Antarctica, received wisdom was that terrestrial

Table 6. Major and minor element concentrations on fused beads determined by laser ablation inductively coupled plasma–mass spectrometry.

Meteorite	ALH 85015	ALHA 77256	EET 83246	GRA 98108	LAP 03979	LEW 88008	LEW 88679	MIL 03368	PCA 02008
Specific	,7	,158	,26	,22	,6	,18	,10	,10	,6
Mass (mg)	347	453	447	500	315	572	369	552	510
SiO_2	48.7	49.7	50.1	47.9	49.4	49.6	49.5	49.5	50.6
TiO_2	0.149	0.126	0.101	0.118	0.124	0.135	0.142	0.095	0.180
Al_2O_3	2.65	1.32	1.02	0.911	2.05	1.80	1.30	0.918	2.15
Cr_2O_3	1.03	0.907	0.985	0.626	0.961	1.03	0.565	1.03	0.906
FeO	17.9	15.8	17.1	17.3	17.3	17.9	17.2	16.6	15.1
MnO	0.571	0.547	0.556	0.557	0.549	0.626	0.565	0.546	0.522
MgO	25.7	28.7	27.2	31.0	25.7	25.1	27.6	28.2	27.7
CaO	2.84	1.42	1.43	1.37	2.37	2.38	1.71	1.55	2.35
Na_2O	0.066	0.006	0.021	0.019	0.062	0.038	0.012	0.019	0.066
Total	99.606	98.526	98.513	99.801	98.516	98.609	98.594	98.458	99.574

alteration would be insignificant. Nevertheless, analyses of eucrites revealed anomalous rare earth element (REE) patterns that were attributed to the effects of low-temperature alteration suffered while in Antarctica (Mittlefehldt and Lindstrom 1991). One key characteristic of altered eucrites is anomalous Ce contents; anomalously high Ce is often associated with low light REE (LREE) samples and anomalously low Ce is associated with samples that have high LREE contents (Mittlefehldt and Lindstrom 1991, 2003). The hypothesis proposed to explain these anomalies is that melt-water solutions in the Antarctic environment dissolve REE-rich phosphates and locally redistribute the REE within the rock. Because Ce can be oxidized to Ce^{4+}, which is less soluble, it becomes partially decoupled from the REE^{3+}, resulting in the observed Ce anomalies (Mittlefehldt and Lindstrom 1991).

Previous compositional studies of diogenites at JSC were carried out by INAA (Mittlefehldt 1994, 2000), and Ce in these meteorites is below detection by this technique. Thus, Ce anomalies caused by Antarctic alteration could not be identified. Solution ICP-MS is more sensitive for Ce and yields precise and accurate analyses of the LREE for most diogenites.

We have computed the Ce/Ce* ratios for the diogenites studied here, and find two that have anomalous ratios. (The calculated Ce* is the Ce content expected from interpolation of the LREE pattern.) The samples of EET 83246 have an average Ce/Ce* of 1.22, whereas the samples of LEW 88008 have an average Ce/Ce* of 2.06 (Table 8). These diogenites have likely had their Ce contents enhanced by precipitation from alteration solutions, but we cannot determine whether their REE^{3+} contents have been affected. Both of these diogenites have REE patterns (excluding Ce) that are within the ranges of those samples that have normal Ce/Ce*, and their La/Yb and Hf/Yb ratios fall within diogenite trends (Fig. 4). The Hf contents of HEDs are unaffected by Antarctic alteration (Mittlefehldt and Lindstrom 2003). We think it likely that, excluding Ce, the REE data for these two diogenites are unaffected. Nevertheless, we will not use the REE data for these samples for interpretation of diogenite petrogenesis.

ALH 85015, PCA 02008, and PCA 02017

As noted above, ALH 85015 and PCA 02008 have higher concentrations of the most highly incompatible elements than do the other diogenites we have studied. They have high Na_2O, Al_2O_3, and CaO contents (Fig. 3; Table 6) that reflect their high modal plagioclase contents (Beck and McSween 2010). They also have the highest TiO_2 contents of the diogenites we analyzed by LA-ICP-MS (Fig. 3c). Ilmenite has not been reported from these diogenites (Beck and McSween 2010), and their orthopyroxene Al_2O_3 and TiO_2 contents are within the ranges of other diogenites (Beck and McSween 2010; this work, Table 2).

ALH 85015 is a very small sample; 3.2 g recovered mass (see *Antarctic Meteorite Newsletter*, 9(3), 1986). Although originally classified as a diogenite, it was considered a howardite by Berkley and Boynton (1992). The classification of ALH 85015 was reevaluated and confirmed as a diogenite, but the justification for this included the statement ". . . this is a small sample so limited sections are available. Only one shows eucritic material, so its classification as a diogenite stands" (*Antarctic Meteorite Newsletter*, 33(1), 2010). Based on this statement, ALH 85015 fits the definition of a polymict diogenite (Delaney et al. 1983). Beck and McSween (2010) confirm the presence of small basaltic clasts in this meteorite.

PCA 02008 is one of the diogenites identified as containing two distinct populations of pyroxene, with

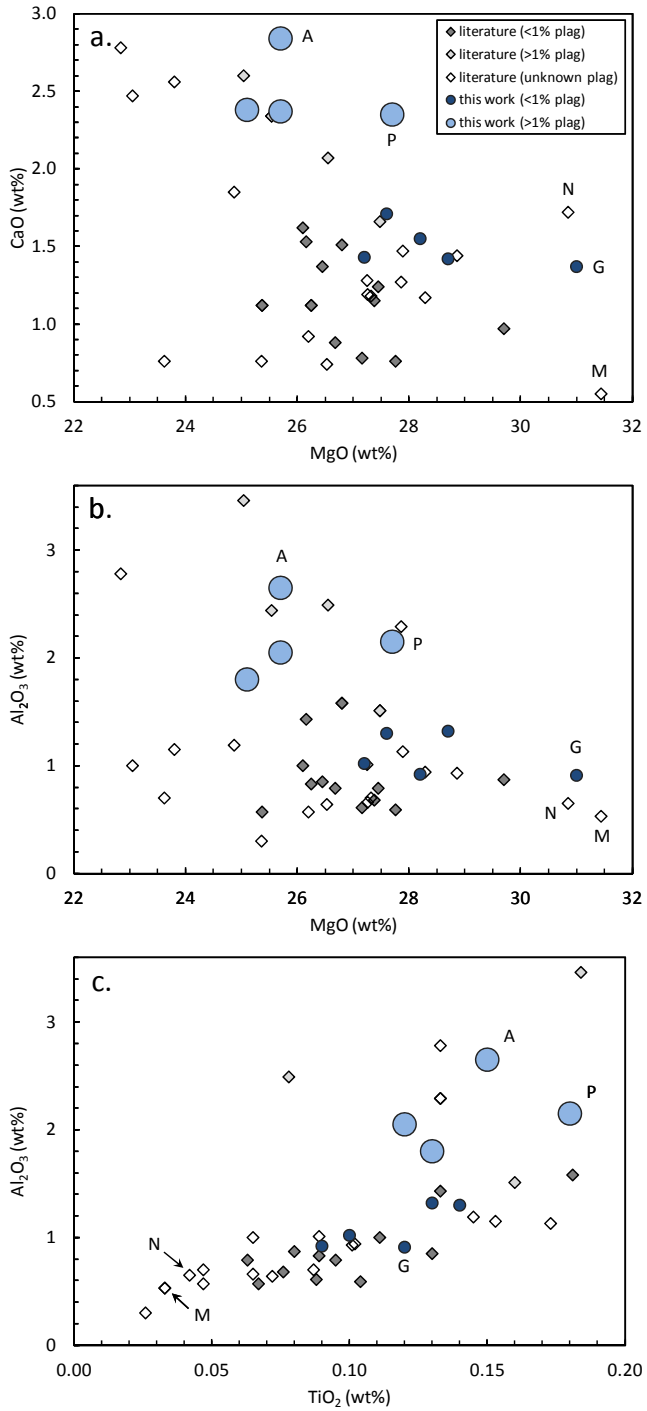

Fig. 3. Major element compositions of diogenites determined by LA-ICP-MS of fused beads in this work compared to literature data on diogenites. Labeled samples are A = ALH 85015, G = GRA 98108, and P = PCA 02008 from this study; M = MET 00425 from Barrat et al. (2008); and N = NWA 1461 from Warren et al. (2009).

mg#s of 78.2 and 75.8 (Beck and McSween 2010). Although it and paired meteorite PCA 02017 are classified as diogenites, cosmogenic nuclide abundances indicate that PCA 02008 is paired with the PCA 02009 howardite pairing group (Welten et al. 2009). Beck and McSween (2010) note the presence of small basaltic clasts in PCA 02008, and we find a small amount of mafic material from cumulate and basaltic eucrite sources in PCA 02017 (see the Results section, and Table 2). Thus, these meteorites are polymict diogenites as defined following Delaney et al. (1983). If these two meteorites are indeed paired with the PCA 02009 howardite, then possibly all should be classified as howardites.

The higher incompatible lithophile element contents of ALH 85015 and PCA 02008 are the result of small amounts of eucritic material admixed into the breccias. The presence of eucritic material would explain the high modal plagioclase contents (Beck and McSween 2010) and consequent high Na_2O, Al_2O_3, and CaO concentrations, and ilmenite-bearing eucritic debris would enhance the TiO_2 concentrations (Fig. 3; Table 6). Figure 4 shows La versus Yb and Hf versus Yb for our analyses (ICP-MS and INAA), the ICP-MS data of Barrat et al. (1999, 2008, 2010) and Beck et al. (2011), and INAA data for Yamato Type B diogenites from Mittlefehldt and Lindstrom (1993). ALH 85015 and PCA 02008 are among the most trace-element-rich, with only five diogenites having comparable or higher La contents. Two of these are Asuka (A)-881838 and A-881839 (Barrat et al. 2008, 2010). These meteorites have similar mineralogy, pyroxene and plagioclase compositions, and bulk rock trace element compositions (Barrat et al. 2008, 2010), and are likely paired (cf. Yamaguchi et al. 2011). Mild leaching with mineral acids removes 75–85% of their La, indicating that phosphate is a major carrier of the LREEs in them (Barrat et al. 2010), and implying that a trapped melt component is included in the cumulate. However, both are rich in Hf (Fig. 4b), which is not appreciably removed by the acid leaching procedure (Barrat et al. 2010). Thus, these diogenites either contain a trapped melt component that carries a significant fraction of the incompatible lithophile elements, or, less likely, they are polymict diogenites with a small eucritic component. In either case, the LREE are mostly contained in phosphate.

MIL 07003 (Barrat et al. 2010) has higher Yb and similar La and Hf concentrations as ALH 85015 and PCA 02008. MIL 07003 is a ferroan, plagioclase-bearing diogenite that appears to be intermediate between classic diogenites and cumulate eucrites (*Antarctic Meteorite Newsletter*, 31(2), 2008). It may be similar in petrogenesis to the Yamato Type B diogenites that are thought to be mesocumulates from melts that were more evolved than typical diogenite parent melts (Mittlefehldt and Lindstrom 1993). Regardless, MIL 07003 is not directly comparable to typical, magnesian diogenites.

Table 7. Whole rock, and orthopyroxene and clast separate compositions determined by instrumental neutron activation analysis.

Meteorite	Bilanga	EET 83247	EET 83247	EET 83247	GRA 98108	GRO 95555	GRO 95555	LAP 91900	LAP 91900	LAP 91900	LAP 91900
Split	,3f,3	,20	,21	,16	,11	,10	,17	,9a	,9b	,10	,29
Type	wr	opx	opx	wr[1]	wr	wr	wr	opx	opx	wr	wr
Mass (mg)	104.67	31.65	15.23	83.22	117.11	102.38	112.94	155.80	180.89	157.52	44.09
Na (μg g^{-1})	81	670	66	339	162	134	141	107	112	71	83
K (μg g^{-1})	110	360			38	34	11	30	70		
Ca (mg g^{-1})	6.5	6.3	4.7	13.6	6.6	8.2	9.5	7.4	7.8	7.9	6.4
Sc (μg g^{-1})	9.84	11.6	10.9	13.8	9.54	11.9	11.7	13.8	13.8	13.8	13.3
Cr (mg g^{-1})	6.01	6.28	4.47	8.35	3.58	7.02	7.07	5.27	5.31	5.29	4.99
Fe (mg g^{-1})	98.9	127	125	129	170	125	123	123	122	121	120
Co (μg g^{-1})	21.6	14.0	19.1	19.1	19.9	14.8	15.7	11.1	12.2	9.71	10.5
Ni (μg g^{-1})	20			50	26			13	17	15	
Se (ng g^{-1})		620	970	1200	790	230	270	190	220	160	
Br (ng g^{-1})	160			56							
La (ng g^{-1})	36	49	15	74	75	15	22	6	10	4	9
Ce (ng g^{-1})											
Sm (ng g^{-1})	68	16	15	78	84	17	25	19	20	21	20
Eu (ng g^{-1})	10			20	18	2.7	5.6	3		2	
Tb (ng g^{-1})	23	20		25	25			9	8	8	
Yb (ng g^{-1})	149	70	70	170	180	88	93	85	80	82	88
Lu (ng g^{-1})	24	13	10	28	29	20	17	16	15	17	20
Hf (ng g^{-1})	60			60	77			30	40		

Meteorite	LEW 88679	LEW 88679	MET 00422	MET 00424	MET 00425	MET 00436	MET 00436	MET 001060	PCA 91077	QUE 93009	QUE 93009
Split	,6	,6	,6	,10	,6	,13	,9	,4	,4	,8a	,8b
Type	opx	wr	wr	wr	wr	wr	wr	wr	wr[2]	clast[3]	wr[4]
Mass (mg)	65.18	46.51	103.82	107.25	97.19	100.45	101.31	141.07	160.29	40.48	125.24
Na (μg g^{-1})	107	189	23	29	59	28	22	8	96	366	877
K (μg g^{-1})					17					20	60
Ca (mg g^{-1})	11	12	5.3	4.2	4.4	4.1	5	3.1	9.4	18	26
Sc (μg g^{-1})	23.0	23.0	15.9	16.7	7.28	16.3	16.5	11.6	14.3	19.8	19.8
Cr (mg g^{-1})	4.57	4.26	6.19	7.47	5.15	12.8	16.0	11.4	5.77	5.76	5.52
Fe (mg g^{-1})	129	128	134	152	88.8	152	154	149	121	145	139
Co (μg g^{-1})	9.87	10.1	22.8	35.8	9.54	14.3	17.6	59.0	17	14.7	13.6
Ni (μg g^{-1})	20							50	36		
Se (ng g^{-1})	600	690		1100	390	1100	790	3400	100		170
Br (ng g^{-1})					38						
La (ng g^{-1})	9	16	3	5	15	9	6	28	13	460	1140
Ce (ng g^{-1})										2000	3600
Sm (ng g^{-1})	93	96	5		31	12	12		30	411	726
Eu (ng g^{-1})	14	29			3			3	5	58	164
Tb (ng g^{-1})	48	46			12				14	134	185
Yb (ng g^{-1})	390	390	41		94	40	30	30	152	730	820
Lu (ng g^{-1})	62	61	10		16	4	5	7	25	112	124
Hf (ng g^{-1})	120	120			51				20	320	570

Note: Missing data were not detected.
[1]Data repeated from Mittlefehldt (1994); includes Ir = 2.8 ± 0.4 ng g–1.
[2]Includes Ir = 0.8 ± 0.2 ng g^{-1}.
[3]Includes Ta = 41 ± 5 ng g^{-1}.
[4]Includes Sr = 18 ± 8 μg g^{-1}, Zr = 20 ± 7 μg g^{-1}, Ta = 67 ± 4 ng g^{-1}, Th = 106 ± 27 ng g^{-1}.

Table 8. Whole rock compositions determined by solution inductively coupled plasma–mass spectrometry.

Meteorite	EET 83246	EET 83246	LAP 03979	LAP 03979	LEW 88008	LEW 88008	LEW 88679	LEW 88679	MET 01084	MET 01084
Specific	,26 (a)	,26 (c)	,6 (a)	,6 (c)	,18 (a)	,18 (c)	,10 (a)	,10 (c)	,8 (a)	,8 (c)
Type	Dimict	Dimict	Dimict	Dimict	Dimict	Dimict	Dimict	Dimict	Dimict	Dimict
Mass (mg)	68.58	67.80	64.44	60.00	65.14	62.74	67.11	49.10	69.34	59.68
Li (μg g^{-1})	4.56	3.65	1.99	1.89	2.19	1.97	1.66	0.836	2.86	2.54
Be (ng g^{-1})			30.4		36.9				36.5	
Na (μg g^{-1})	106	149	379	497	249	276	72.8	101	183	234
Al (mg g^{-1})	4.60	5.81	11.6	14.5	10.3	10.4	7.54	6.95	8.50	10.4
P (μg g^{-1})	4.98	5.72	18.8	23.1	10.1	13.7	6.82	9.42	32.4	34.7
Ca (mg g^{-1})	9.82	9.90	18.0	19.1	18.1	15.9	13.0	12.1	12.8	12.7
Sc (μg g^{-1})	11.1	13.5	14.3	19	20.7	20.1	20.3	16	13.8	16.6
Ti (mg g^{-1})	0.640	0.641	0.819	0.981	0.855	0.858	0.950	0.908	1.01	1.07
V (μg g^{-1})	94.6	116	120	147	147	142	116	90.5	82.6	101
Cr (mg g^{-1})	5.92	5.90	6.38	7.62	7.53	5.85	3.05	3.32	4.21	3.99
Mn (mg g^{-1})	4.00	4.32	4.03	4.87	4.78	4.71	4.12	4.36	3.64	3.96
Fe (mg g^{-1})	109	130	125	151	148	142	143	143	116	129
Co (μg g^{-1})	15.8	16.5	23.1	26.4	16.0	16.9	19.1	21.2	17.3	18.7
Ni (μg g^{-1})	28.5	34.5	137	168	31.1	36.9	31.3	38.2	49.9	62.6
Cu (μg g^{-1})	2.45	1.66	3.91	5.42	3.20	4.09	8.63	9.93	4.36	3.24
Zn (μg g^{-1})	5.86	4.51	4.22	5.63	2.54	5.95	6.16	5.99	4.60	5.58
Ga (μg g^{-1})	0.506	0.690	0.562	0.919	0.506	0.791	0.589	0.736	0.517	0.788
Ge (ng g^{-1})		150		217		210		248		168
Rb (ng g^{-1})	75.5	100	33.9	79.4	147	120	35.6	56.2	44.2	78.2
Sr (μg g^{-1})	1.63	1.51	6.78	7.49	3.64	3.61	1.30	1.33	4.26	4.03
Y (μg g^{-1})	1.23	1.17	1.91	2.11	1.95	2.00	2.52	1.94	3.11	3.24
Zr (μg g^{-1})	3.00	2.14	4.45	6.23	4.22	2.84	2.81	2.20	5.82	7.18
Nb (ng g^{-1})	127	114	288	281	165	132	54.6	50.2	339	349
Cs (ng g^{-1})	2.6	2.1	1.7	2.1	4.3	4.1	1.4		3.1	2.7
Ba (μg g^{-1})	0.635	0.495	1.55	1.60	1.50	1.46	0.128		1.47	1.22
La (ng g^{-1})	67.8	62.9	145	158	87.6	91.1	7.50	5.00	168	206
Ce (ng g^{-1})	212	198	379	412	501	519	32.0	24.1	475	540
Pr (ng g^{-1})	25.2	23.1	59.7	62.9	38.5	38.3	8.80	6.70	81.1	87.0
Nd (ng g^{-1})	140	124	316	332	217	214	84.6	63.3	470	487
Sm (ng g^{-1})	58.3	54.2	118	123	94.7	92.2	79.1	60.1	196	199
Eu (ng $g^{-1)}$	7.8	8.5	45.7	54.6	18.8	22.3	7.8	9.5	34.4	38.7
Gd (ng g^{-1})	98.6	90.0	180	189	164	159	181	136	308	306
Tb (ng g^{-1})	20.3	18.3	35.1	37.8	33.2	33.7	40.1	30.1	59.2	59.8
Dy (ng g^{-1})	157	144	261	276	258	258	327	240	435	438
Ho (ng g^{-1})	41.9	38.6	66.1	70.9	68.9	67.4	86.5	65.6	108	109
Er (ng g^{-1})	143	134	217	229	226	224	293	217	338	341
Tm (ng g^{-1})	25.2	22.6	35.4	37.8	38.2	37.4	48.2	35.7	54.7	55.4
Yb (ng g^{-1})	166	162	233	258	277	263	329	250	354	366
Lu (ng g^{-1})	28.7	26.9	39.5	42.3	43.5	42.2	53.8	39.7	56.8	59.0

Table 8. *Continued.* Whole rock compositions determined by solution inductively coupled plasma–mass spectrometry.

Meteorite	EET 83246	EET 83246	LAP 03979	LAP 03979	LEW 88008	LEW 88008	LEW 88679	LEW 88679	MET 01084	MET 01084
Specific	,26 (a)	,26 (c)	,6 (a)	,6 (c)	,18 (a)	,18 (c)	,10 (a)	,10 (c)	,8 (a)	,8 (c)
Type	Dimict	Dimict	Dimict	Dimict	Dimict	Dimict	Dimict	Dimict	Dimict	Dimict
Hf (ng g^{-1})	88.8	57.2	116	154	106	80.2	97.9	77.0	183	185
Ta (ng $g^{-1)}$	4.8	5.6	10.8	12.7	5.5	6.0	1.7	1.8	13.1	15.1
Tl (ng g^{-1})	7.7	7.4	0.6	0.6	65.4	69.4	6.7	7.2	2.3	2.2
Pb (ng g^{-1})	85.8	55.3	103	30.0	494	635		20.5	113	22.8
Th (ng g^{-1})	11.1	10.9	18.8	20.9	23.3	23.5	0.5	1.4	21.3	27.0
U (ng g^{-1})	2.6	2.7	6.3	5.7	10.6	10.8	1.4	1.5	7.8	8.1
Eu/Eu*	0.317	0.376	0.972	1.109	0.465	0.568	0.196	0.316	0.433	0.486
Ce/Ce*	1.211	1.226	0.962	0.976	2.036	2.075	0.811	0.828	0.957	0.953
Meteorite	MIL 03368	MIL 03368	ALHA77256	ALHA77256	GRA 98108	GRA 98108	ALH 85015	ALH 85015	PCA 02008	PCA 02008
Specific	,10 (a)	,10 (c)	,158 (a)	,158 (c)	,22 (b)	,22 (c)	,7 (a)	,7 (c)	,6 (b)	,6 (c)
Type	Dimict	Dimict	Harzburgitic	Harzburgitic	Harzburgitic	Harzburgitic	Polymict	Polymict	Polymict	Polymict
Mass (mg)	63.69	59.34	65.49	61.18	66.70	64.51	69.14	49.43	67.40	65.97
Li (μg g^{-1})	3.31	3.18	1.82	1.63	3.00	1.45	3.37	3.24	3.65	3.34
Be (ng g^{-1})			28.7				36.1		45.4	
Na (μg g^{-1})	133	165	80.5	38.2	101	130	431	508	433	467
Al (mg g^{-1})	4.27	5.60	6.28	8.14	4.24	4.11	14.5	16.5	11.8	13.3
P (μg g^{-1})	15.0	3.13	9.88	10.3	26.5	27.6	48.2	55.7	50.9	55.7
Ca (mg g^{-1})	11.6	10.9	10.6	10.3	8.79	8.30	19.1	19.1	15.9	15.6
Sc (μg g^{-1})	10.9	13.7	15.7	18.9	14.4	11.3	14.5	16.1	14.9	15.9
Ti (mg g^{-1})	0.626	0.626	0.803	0.814	0.759	0.671	0.839	0.843	1.06	1.13
V (μg g^{-1})	144	172	122	149	143	137	116	122	98.7	105
Cr (mg g^{-1})	6.03	6.18	6.09	5.47	4.65	3.79	6.43	6.63	5.66	4.40
Mn (mg g^{-1})	3.77	4.26	3.91	4.13	3.82	4.00	4.02	4.39	3.75	3.96
Fe (mg g^{-1})	123	133	114	126	125	131	133	144	120	127
Co (μg g^{-1})	21.5	21.9	10.7	12.8	13.4	14.5	24.5	27.7	21.8	21.8
Ni (μg g^{-1})	11.2	12.2	9.92	12.6	17.4	19.7	130	979	118	144
Cu (μg g^{-1})	3.87	4.49	2.73	3.16	3.48	2.89	5.68	9.40	2.73	3.53
Zn (μg g^{-1})	13.3	3.88	8.30	4.88	5.19	3.77	6.24	5.91	6.37	5.51
Ga (μg g^{-1})	0.407	0.655	0.536	0.814	0.473	0.723	0.817	1.14	0.760	1.04
Ge (ng g^{-1})		170		190		205		280		209
Rb (ng g^{-1})	41.2	63.1	14.8	29.1	37.7	54.8	39.0	80.2	36.0	63.5
Sr (μg g^{-1})	0.396	0.299	0.674	0.341	0.405	0.319	11.0	10.7	11.1	8.66
Y (μg g^{-1})	1.00	1.04	1.84	1.88	2.43	2.06	2.22	2.29	3.71	3.87
Zr (μg g^{-1})	0.680	0.777	4.59	3.63	4.82	3.71	5.77	6.21	8.02	8.83
Nb (ng g^{-1})	62.3	49.9	335	329	205	189	426	402	534	588
Cs (ng g^{-1})	3.5	1.8	11.9		2.5	2.1	1.5	1.6	2.0	1.3
Ba (μg g^{-1})	0.0968		0.789		0.0839	0.0332	3.46	3.21	4.06	3.84
La (ng g^{-1})	19.6	15.5	110	136	50.9	43.8	279	289	471	521
Ce (ng g^{-1})	50.7	41.9	294	330	210	175	705	717	1170	1250
Pr (ng g^{-1})	8.5	9.1	40.3	43.5	44.4	38.4	107	106	179	192

Table 8. *Continued.* Whole rock compositions determined by solution inductively coupled plasma–mass spectrometry.

Meteorite	MIL 03368	MIL 03368	ALHA77256	ALHA77256	GRA 98108	GRA 98108	ALH 85015	ALH 85015	PCA 02008	PCA 02008
Specific	,10 (a)	,10 (c)	,158 (a)	,158 (c)	,22 (b)	,22 (c)	,7 (a)	,7 (c)	,6 (b)	,6 (c)
Type	Dimict	Dimict	Harzburgitic	Harzburgitic	Harzburgitic	Harzburgitic	Polymict	Polymict	Polymict	Polymict
Nd (ng g^{-1})	49.3	59.7	215	227	305	258	546	537	934	988
Sm (ng g^{-1})	28.0	27.8	84.5	84.6	155	129	182	175	309	321
Eu (ng g^{-1})	1.5	3.2	6.0	7.5	1.5	2.4	79.9	83.6	75.1	77.3
Gd (ng g^{-1})	60.2	61.6	144	145	244	206	255	245	428	448
Tb (ng g^{-1})	13.9	14.3	30.2	30.2	47.8	40.4	46.4	45.7	79.4	80.9
Dy (ng g^{-1})	119	121	238	236	338	288	326	319	536	546
Ho (ng g^{-1})	34.0	34.6	62.3	62.6	83.7	71.2	78.1	78.1	127	129
Er (ng g^{-1})	122	124	210	211	267	226	248	247	389	397
Tm (ng g^{-1})	21.7	21.5	34.2	34.9	42.9	36.6	39.8	40.1	60.3	59.9
Yb (ng g^{-1})	146	161	231	237	286	247	271	273	388	396
Lu (ng g^{-1})	26.7	27.5	38.4	39.0	46.8	39.9	43.5	43.2	61.4	61.5
Hf (ng g^{-1})	20.4	24.4	138	96.2	141	100	149	152	211	221
Ta (ng g^{-1})	0.9	1.9	8.2	8.3	8.6	8.9	18.4	20.6	25.7	28.8
Tl (ng g^{-1})	4.7	4.4	2.1	0.9	3.4	3.7	0.5	0.8	2.4	2.5
Pb (ng g^{-1})	36.6		75.9		24.7	94.1	32.0	75.6	308	103
Th (ng g^{-1})	3.9	2.3	14.2	16.2	16.6	10.0	36.4	34.6	57.7	61.4
U (ng g^{-1})	2.3	1.7	6.5	6.1	5.0	4.7	10.7	10.9	15.2	15.6
Eu/Eu*	0.111	0.233	0.168	0.209	0.024	0.046	1.151	1.253	0.641	0.633
Ce/Ce*	0.927	0.818	1.042	1.007	0.969	0.935	0.964	0.967	0.952	0.933

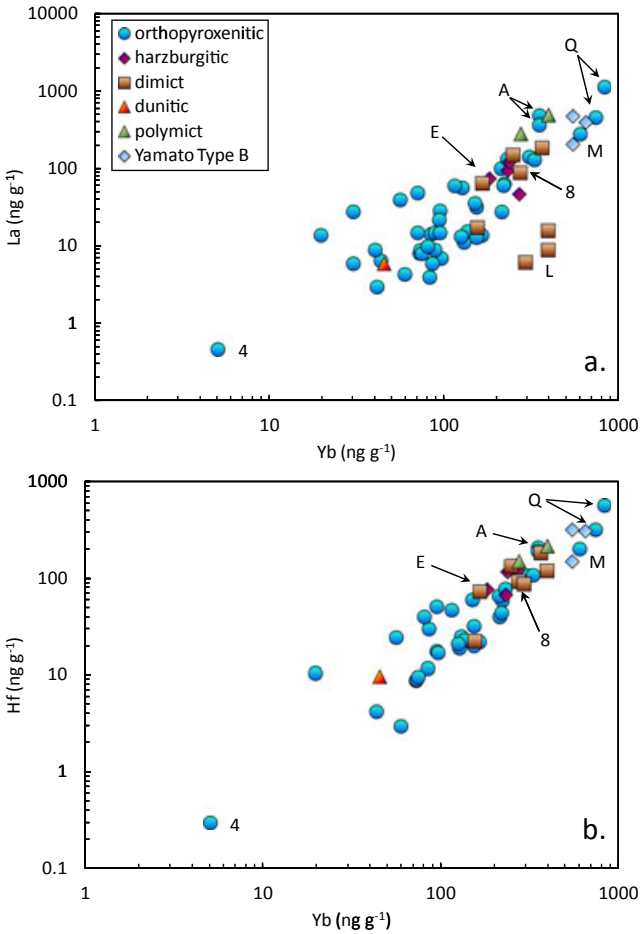

Fig. 4. La versus Yb (a) and Hf versus Yb (b) for the diogenites studied here and literature analyses. Nomenclature modified from Beck and McSween (2010) (see text). Labeled diogenites are E = EET 83246, L = LEW 88679, 8 = LEW 88008, and Q = QUE 93009 from this work; and A = A-881838 and A-881839, 4 = MET 00424, and M = MIL 07001 from Barrat et al. (2010). Other literature data are from Barrat et al. (1999, 2008, 2010), Beck et al. (2011), and Mittlefehldt and Lindstrom (1993).

QUE 93009

QUE 93009 is the most incompatible-element-rich diogenite shown in Fig. 4. We analyzed a bulk rock sample and a clast separate (Table 7). The high trace element contents of the clast sample (lower of the two on Fig. 4) cannot be due to eucritic contamination. As noted above, the clast separate is rich in Na, and noritic clasts composed of intergrown, coarse (milimeter-sized) plagioclase, and orthopyroxene are present in this meteorite. Plagioclase also occurs as mineral fragments in the matrix, but these are not associated with eucritic pyroxenes. Pyroxenes in QUE 93009 are on the ferroan side of the range of typical diogenite orthopyroxene compositions (Fig. 1), and on average, have higher TiO_2 contents (Table 2) (Fowler et al. 1994; Mittlefehldt 1994). However, QUE 93009 pyroxenes are more magnesian than those of cumulate eucrites. We found no petrologic evidence for a eucritic component in this breccia. Thus, it is not a polymict diogenite in the sense of Delaney et al. (1983).

Pyroxenes in QUE 93009 are less ferroan than those of Yamato Type B diogenites (Fig. 1). QUE 93009 contains ilmenite, which has been previously reported only in Yamato Type B diogenites (Mittlefehldt and Lindstrom 1993). Ilmenite occurs as exsolutions in chromite grains in QUE 93009, whereas in Y-75032 and Y-791199 ilmenite occurs as a discrete phase. Thus, QUE 93009 shows some petrologic similarities to the Yamato Type B diogenites, but is richer in incompatible trace elements than the latter (Fig. 4).

We found no petrologic evidence that QUE 93009 contains a significant trapped melt component. The clast and bulk samples have Eu/Eu* of 0.34 and 0.60, and for this reason, if the norite clasts are cumulates, they cannot dominate the incompatible trace element budget of the rocks; norite cumulates would have Eu/Eu* > 1. (The calculated Eu* is the Eu content expected from interpolation of a REE pattern.) QUE 93009 plausibly represents a transitional rock type between typical diogenites and magnesian cumulate eucrites such as Binda. Binda is a polymict cumulate eucrite (Delaney et al. 1983) with the cumulate component containing 70–75 vol% pyroxene (Duke and Silver 1967; Delaney et al. 1984) with a primary (pre-exsolution) mg# of approximately 67 (Takeda et al. 1976). Yamato Type B diogenites are also considered to be intermediate between diogenites and cumulate eucrites (Takeda and Mori 1985; Mittlefehldt and Lindstrom 1993).

LEW 88679

LEW 88679 is one of several diogenites identified by Beck and McSween (2010) as containing two distinct lithologies, a more magnesian harzburgite and a more ferroan orthopyroxenite. Plagioclase occurs in both lithologies. This diogenite stands out on Fig. 4a as having a lower La/Yb ratio than any other diogenite. The REE data for LEW 88679 are shown in Fig. 5 and compared to orthopyroxene/melt K_Ds from Schwandt and McKay (1998) (their spot 3, $Wo_{1.2}$ pyroxene). For this partition coefficient set, D_{Gd} is interpolated and the Eu partition coefficient is scaled for an assumed fO_2 of one log unit below the iron-wüstite (IW) buffer using the D_{Eu}/D_{Gd} relationship of McKay et al. (1990). The orthopyroxene/melt partition coefficients were adjusted to match the heavy REE (HREE) abundances of our ICP-MS analyses at Yb, with all other REE being scaled accordingly.

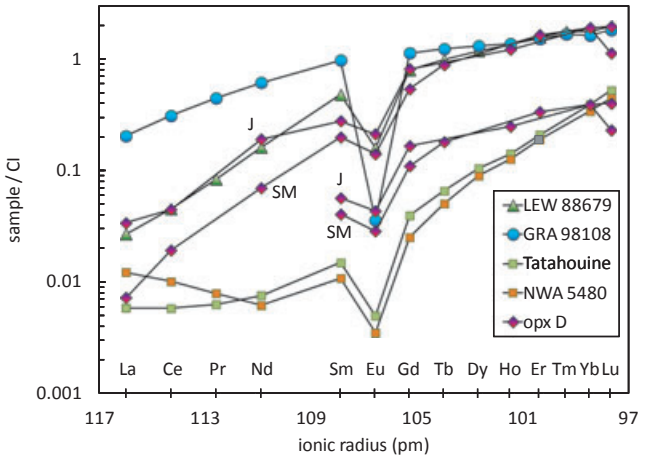

Fig. 5. Rare earth element diagram for GRA 98108 and LEW 88679 (our ICP-MS data) compared to two orthopyroxene/melt distribution coefficient sets; J calculated after Jones (1995) and SM from Schwandt and McKay (1998). Comparative data for NWA 5480 and Tatahouine from Barrat et al. (1999, 2010) are shown, compared to the same orthopyroxene/melt partition coefficients (Sm through Lu only) scaled to lower absolute values. See text for details of how partition coefficients were calculated and scaled.

Although LEW 88679 has a lower La/Yb ratio than any other diogenite, it nevertheless could contain a small amount of a trapped melt component. The LREE contents of LEW 88679 are higher than expected for a pure orthopyroxene cumulate if the partition coefficients of Schwandt and McKay (1998) are appropriate and assuming that the parent melt had chondritic-relative REE ratios. Based on these partition coefficients, only approximately 0.1% of a trapped melt component could explain the difference. Also shown is a partition coefficient set calculated after Jones (1995), using data from his Table 6, and a log D_{Ca} of −0.85 estimated from the modeling of Righter and Drake (1997). This partition coefficient set was also adjusted to match the Yb abundance of LEW 88679. The Jones D set has a higher LREE/HREE ratio, and if these are more applicable, then no trapped melt component is indicated for LEW 88679.

The above discussion was based only on orthopyroxene/melt partitioning, while LEW 88679,8 contains approximately 15 vol% olivine (Beck and McSween 2010). Olivine/melt partition coefficients also show extreme LREE/HREE fractionation, and have lower absolute values than orthopyroxene/melt partition coefficients (cf. McKay 1986; Schwandt and McKay 1998). Using a bulk distribution coefficient set that includes olivine in the calculated cumulate does not alter the conclusion just arrived at, viz. the observed LREE–HREE fractionation could be consistent with LEW 88679 being an orthopyroxene–olivine cumulate sans trapped melt.

LEW 88679 also has anomalously low Nb/Yb, Ta/Yb, Th/Yb, and U/Yb ratios compared to other diogenites we have studied, but has a normal Hf/Yb ratio (Fig. 4b). Orthopyroxene/melt partition coefficients for Nb, La, Th, and U are much lower than for Yb or Hf (Beattie 1993; Schwandt and McKay 1998; Righter and Shearer 2003; Norman et al. 2005); we expect the same is true for Ta. Thus, elements that are most susceptible to enhancement by inclusion of a trapped melt component are low, again suggesting that LEW 88679 may be composed of nearly pure adcumulate harzburgite and orthopyroxenite.

However, to match the partition coefficients with our LEW 88679 data, a parent melt with approximately 24 times (for the Schwandt and McKay partition coefficient set) or approximately 40 times (for the Jones partition coefficient set) CI abundances of REE is required. These are implausibly high for diogenite parent magmas given that primitive eucrites such as Sioux County only have approximately eight times CI REE (e.g., Fukuoka et al. 1977; Mittlefehldt 1979). The situation becomes even worse using partition coefficients calculated after Jones (1995) and the D_{Ca} recovered from the Schwandt and McKay (1998) experiments, and/or by including olivine as a cumulus phase. Thus, although we can match the REE *pattern* of LEW 88679 quite successfully with existing partition coefficient *ratios*, the absolute concentrations are difficult to explain by this simple model. As the absolute values of the low-Ca pyroxene/melt partition coefficients increase, the La/Yb ratios also increase (e.g., Jones 1995; Bédard 2007). We cannot get relief from our quandary by appealing to vague uncertainties in partitioning.

As mentioned, LEW 88679 is a dimict breccia of magnesian harzburgite and ferroan orthopyroxenite (Beck and McSween 2010). Even if they represented different parts of the same intrusion, it is unlikely that both would be devoid of a trapped melt component. It is more likely that the anomalously low trace element contents of LEW 88679 were rather developed after impact mixing of the two lithologies by some process acting on the breccia. Beck and McSween (2010) suggested that postcrystallization metamorphic equilibration acting on distinct lithologies of a single pluton might explain the pyroxene minor element contents of LEW 88679. This scenario may be consistent with the anomalously low concentrations of highly incompatible elements in this diogenite, and could be explored through in situ trace element analyses.

We analyzed bulk samples of LEW 88679, i.e., mixtures of harzburgite and orthopyroxenite, and it is thus possible that one of the two lithologic components is similar to most diogenites in its highly incompatible lithophile element contents, whereas the other is

extremely poor in such elements. Beck and McSween (2010) noted that the modal abundance of olivine in their section of LEW 88679 is quite different from that used for the initial description (*Antarctic Meteorite Newsletter*, 15(1), 1992). They concluded that LEW 88679 is heterogeneous in terms of the proportions of the two lithologic components. Our INAA and ICP-MS samples, taken from separate chips, have identical (within 10%) La/Yb ratios. Thus, if the two lithologic components have dramatically different trace element signatures, then our two samples must have had roughly the same proportions of these components. This seems unlikely but is not impossible. We favor the scenario where the anomalous trace element contents were engendered by some postbrecciation process that mobilized highly incompatible trace lithophile elements, but this hypothesis requires testing through detailed petrologic and in situ trace element investigation. Because orthopyroxenes with distinct mg# are present in this rock (Beck and McSween 2010), this process was not the thermal metamorphism that decoupled Fe-Mg from minor/trace element concentrations generally in diogenites (Mittlefehldt 1994).

Petrogenesis

Although broad-scale differentiation models for Vesta can explain the first-order mineralogy, mineral compositions, and bulk major element compositions of diogenites (e.g., Righter and Drake 1997; Ruzicka et al. 1997; Warren 1997), they do not explain the details of minor and trace element distributions (Mittlefehldt 1994). As a result, models for the petrogenesis of diogenites have been at odds with the broad-scale models for eucrite genesis (Mittlefehldt 1994; Fowler et al. 1995; Shearer et al. 1997, 2010).

Tatahouine, NWA 5480, and MET 00424 represent special cases. The normalized REE abundances of Tatahouine increase very steeply from Sm to Lu (Fig. 5). NWA 5480 has a nearly identical pattern for the HREE (Fig. 5) (Barrat et al. 2010). Fukuoka et al. (1977) demonstrated that the steep increase in HREE for Tatahouine cannot be explained as originating in an orthopyroxene cumulate formed from magma with chondritic REE ratios. This remains true when using modern orthopyroxene/melt Ds (Jones 1995; Schwandt and McKay 1998) for the modeling (Fig. 5). This led to the hypothesis that the parent magma for Tatahouine was formed by remelting of an earlier generation of orthopyroxene cumulates followed by fractional crystallization to form a second-generation cumulate (Fukuoka et al. 1977). These authors also noted that Tatahouine could be a melting residue of an early generation of orthopyroxene cumulates. This hypothesis was reiterated by Mittlefehldt (1994), and should apply to NWA 5480 as well (Barrat et al. 2010). The cumulate remelting model was extended by Barrat et al. (2008) to include MET 00424, the diogenite with the lowest concentrations of incompatible lithophile elements (Mittlefehldt 2002; Barrat et al. 2008, 2010). The chondrite-normalized Sm/Lu ratio of MET 00424 is approximately 0.004, compared to that of Tatahouine of 0.028 (Barrat et al. 2010). The origin of the REE pattern of MET 00424 is challenging to model (see Barrat et al. 2010, p. 6225), but these authors state that generation of the pattern includes ". . . a strongly heavy REE enriched component (i.e., a pure orthopyroxenite) . . ." by which we presume they mean that a cumulate remelting process is required.

Expanding on Fukuoka et al. (1977), Barrat et al. (2008) have concluded that rather than being cumulates from earlier in the crystallization sequence of a molten Vesta, diogenites more generally are cumulates formed from magmas generated by remelting lower crustal cumulates from the initial magma ocean stage. These authors extended their interpretation by noting that the orthopyroxene fraction of some diogenites, prepared by acid leaching of bulk rock samples to remove phosphates, has Eu/Eu* much lower than expected for orthopyroxene in equilibrium with a magma with chondritic REE ratios (Barrat et al. 2010). This led them to conclude that some diogenite parent magmas were contaminated by melts generated by remelting the basaltic (eucritic) crust, and therefore the diogenite parent magmas must be younger than the age of major crust formation on Vesta.

The crux of the argument is illustrated on a plot of Eu versus Gd (Fig. 6) for the leached diogenite residues from Barrat et al. (2010). All diogenites plot below the CI ratio (dashed line) on this diagram and therefore have subchondritic Eu/Gd ratios. Many of the residues plot between the CI ratio line and the line for model orthopyroxene cumulates in equilibrium with melts having CI Eu/Gd ratios. (The Eu and Gd partition coefficients used for this line are those from Barrat et al. (2007) that were used in modeling diogenite petrogenesis by Barrat et al. (2010).) Diogenites that plot near the orthopyroxene cumulate line may have equilibrated with magma with chondritic Eu/Gd. Those that plot between the cumulate and CI ratio lines could represent cumulates with variable amounts of included trapped melt.

A large number of the diogenite residues plot below the cumulate line of Fig. 6. If the Eu partition coefficient used is accurate for the conditions of diogenite formation and diogenites are unmodified igneous cumulates, then those diogenites that plot below the cumulate line must have crystallized from magma with a subchondritic

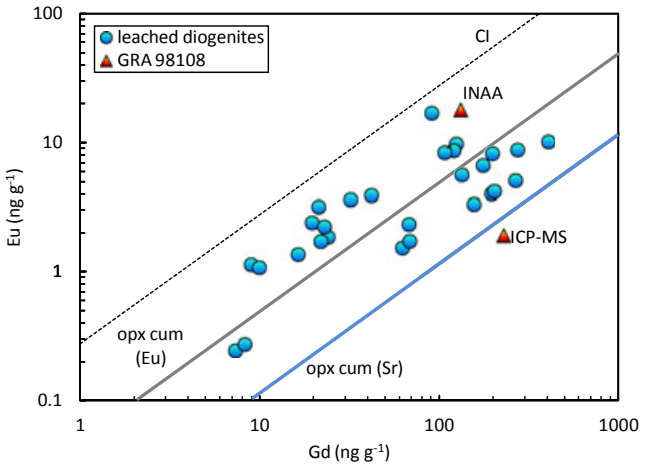

Fig. 6. Eu versus Gd for acid leached diogenites from Barrat et al. (2010) and (untreated) GRA 98108 from this study. Only falls and Antarctic diogenites are plotted. The line labeled opx cum (Eu) is the locus of orthopyroxene in equilibrium with melts with CI Eu/Gd ratios. The line labeled opx cum (Sr) is the locus of orthopyroxene in equilibrium with melts with CI Sr/Gd ratios. The partition coefficients used are from Barrat et al. (2007) and were used by Barrat et al. (2010) to model diogenite genesis (see text for discussion).

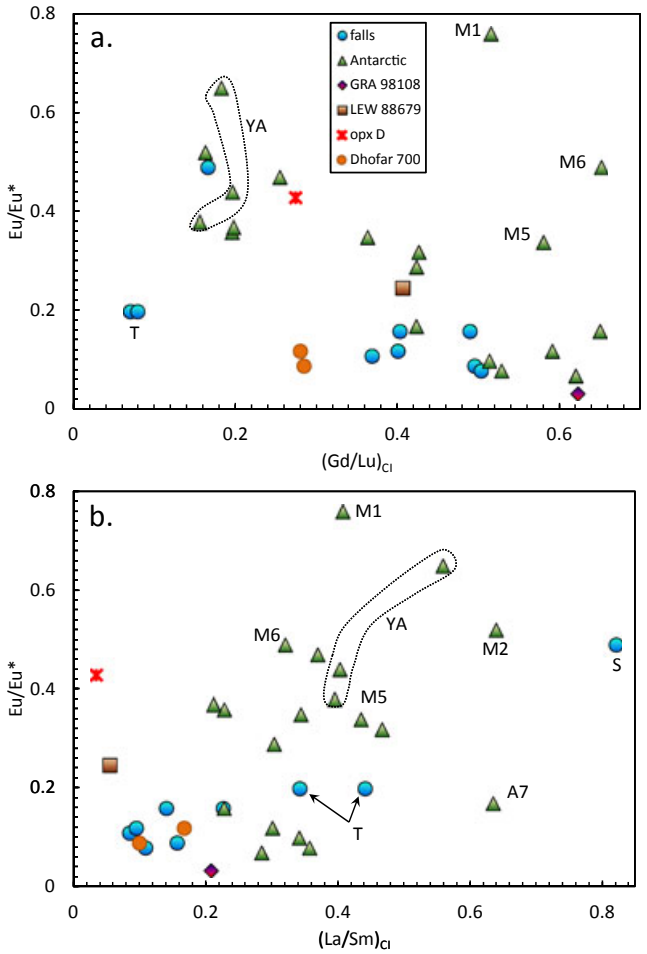

Fig. 7. Eu/Eu* versus Gd/Lu (a) and Eu/Eu* versus La/Sm (b) for leached diogenites from Barrat et al. (2010) compared to unleached GRA 98108 and LEW 88679 from this study. Opx *D* is the orthopyroxene/melt partition coefficient set of Schwandt and McKay (1998). Labeled diogenites are A7 = ALHA77256, M1 = MIL 07001, M2 = MET 00422, M5 = MET 00425, M6 = MET 00436, S = Shalka, T = Tatahouine, and YA = paired Yamato Type A diogenites Y-74013 and Y-74097.

Eu/Gd ratio, as advocated by Barrat et al. (2010). For comparison, a model cumulate based on the Sr partition coefficient is shown. The partitioning behavior of Eu^{2+} is very similar to that of Sr^{2+} (Drake and Weill 1975). Thus, the model cumulate line based on Sr is the absolute limit for orthopyroxene cumulates in equilibrium with magma with chondrite Eu/Gd under conditions so reducing that all Eu is divalent. Also shown on Fig. 6 are our data for harzburgitic diogenite GRA 98108.

Barrat et al. (2010) show that a partial melt of basaltic eucrite crustal rock would have a subchondritic Eu/Gd ratio because the anatectic residue would be a mixture of low-Ca pyroxene and plagioclase; Eu^{2+} is compatible in plagioclase (Drake and Weill 1975). Mixing this crustal melt with a penultimate diogenite parent melt that has a chondritic Eu/Gd ratio would produce the ultimate diogenite parent melt with subchondritic Eu/Gd as suggested by Fig. 6. The model of Barrat et al. (2010) is thus that diogenites crystallized from magmas produced by remelting early magma ocean cumulates, some of which were contaminated by partial melts of the eucritic crust of Vesta.

The crustal melt also has superchondritic Gd/Lu and La/Sm that will be inversely correlated with Eu/Eu* (see fig. 11 of Barrat et al. 2010). In a simple model for formation of diogenites from mixed-magmas, one would expect that the derived ultramafic cumulates (harzburgites, orthopyroxenites) should express an inverse correlation between Eu/Eu* and Gd/Lu. In gross detail, this is what is observed (Fig. 7a). Excluding a few outliers, there is a good general trend of decreasing Eu/Eu* with increasing $(Gd/Lu)_{CI}$ that qualitatively matches expectations from Barrat et al.'s (2010) hypothesis. Several diogenites plot close to the orthopyroxene/melt *D* ratios (those with slightly lower $(Gd/Lu)_{CI}$ and similar Eu/Eu*). These are plausible cumulates from parent melts that were not contaminated by crustal melts. Because these melts plot close to the orthopyroxene/melt *D* ratios, their parent melts may have had chondritic-relative REE ratios, that is, they were not liquids produced by remelting magma ocean cumulates. The unlabeled points with higher $(Gd/Lu)_{CI}$ than the orthopyroxene partition

coefficient are plausible cumulates from parent melts that had been contaminated by crustal melts. Based on their position in Fig. 7a, LEW 88679 and GRA 98108 are consistent with an origin as cumulates derived from magmas contaminated by crustal melts.

Tatahouine has an anomalously low Sm abundance compared to its HREE abundances and is consistent with being a restite from orthopyroxenite cumulate melting, or a cumulate formed from magmas produced by remelting orthopyroxenitic cumulates (Fukuoka et al. 1977). The low $(Gd/Lu)_{CI}$ and Eu/Eu* ratios for Tatahouine (Fig. 7a) can be modeled by either process. Contamination of the Tatahouine parent magma by crustal melts is not required to model the REE pattern of this diogenite.

Barrat et al. (2010) group MET 00425, MET 00436, and MIL 07001 into a compositional subtype of diogenites by virtue of their similar REE patterns, excluding their Eu/Eu*, but do not specifically address their genesis. Figure 7a indicates that these three diogenites, especially MIL 07001, have trace element characteristics that suggest they may be cumulates plus trapped melt, but that their parent magma did not assimilate crustal melts. MET 00425 is one of the most magnesian diogenites (Mittlefehldt 2002; Barrat et al. 2008). Because of its high mg#, it is not easily fit into generalized models for diogenite genesis.

The expected inverse relationship between Eu/Eu* and La/Sm is not observed, however (Fig. 7b). Many of those diogenites with the lowest Eu/Eu* and highest Gd/Lu (Fig. 7a) have among the lowest La/Sm (Fig. 7b). If any relationship is present, it is an increase in Eu/Eu* with increasing La/Sm, not the expected decrease. Cumulates formed from contaminated magmas à la Barrat et al. (2010), regardless of whether they contain a trapped melt component, ought to exhibit a distribution on Fig. 7b similar to that in Fig. 7a because of the higher La/Sm ratios of contaminated magmas (cf. Barrat et al. 2010, fig. 11). For this reason, we find the geochemical data do not provide compelling evidence that a substantial number of diogenites were formed from remelted cumulates, or that contamination of diogenitic precursor magmas by partial melts of the basaltic crust was a common process. Nevertheless, the very low Eu/Eu* for some leached diogenites is an anomaly that does not obviously fit into the common model for formation of diogenites as cumulates from a vestan magma ocean, as stressed by Barrat et al. (2010).

Mittlefehldt (1994) demonstrated that the major element concentrations of diogenites are decoupled from their trace element concentrations. He further demonstrated that mineral equilibration temperatures for diogenites are several hundred degrees below plausible magmatic crystallization temperatures. Following Lambert and Simmons (1987), Mittlefehldt (1994) posited that the observed decoupling of Fe-Mg from Al, Sc, Ti, and REE was due to differences in mean diffusion distance for Fe-Mg exchange compared to those for minor and trace elements. In this scenario, diffusion homogenizes the orthopyroxene mg# but leaves igneous-derived variation in incompatible lithophile elements (Al, etc.) largely unaffected.

Cherniak and Liang (2007) have studied REE diffusion in natural enstatite in air and in sealed capsules buffered at IW. They found that diffusion of Gd did not change with oxygen fugacity, whereas Eu diffusion was more than an order of magnitude faster at IW than in air, from which they concluded that Eu^{2+} diffusion in pyroxene is faster than for Eu^{3+}. This suggests that a possible alternative to Barrat et al.'s hypothesis for generating low Eu/Eu* in diogenites is that subsolidus diffusive exchange permitted equilibration of Eu^{2+} between orthopyroxene and accessory phases such as plagioclase or phosphate, whereas Eu^{3+} more closely retains its original igneous distribution (cf. Treiman 1996). The leaching procedure of Barrat et al. (2010) must have removed much or all of the Eu-rich phase, which as they noted, implies that it is a phosphate.

There are few reports of phosphates in diogenites because of their rarity and the small size of the grains. Phosphates were first reported in Roda, where they occur as 5–15 μm sized grains of LREE-rich Ca-phosphate enclosed in an approximately 50 × 80 μm diopside grain that abuts Si-Al-K-Ba-rich glass, all located interstitially between orthopyroxene grains (Mittlefehldt 1994). Domanik et al. (2004) describe LREE-rich Ca-phosphate occurrences in Bilanga, where they are associated with diopside, chromite, troilite, plagioclase, and silica. One such occurrence is adjacent to silica-rich mesostasis containing "K-rich needles" that are similar in composition to the Si-Al-K-Ba-rich glass from Roda (Domanik et al. 2004). These authors mention that X-ray mapping evidence indicates that chemical exchange of P occurred between phases in the region they describe, and infer the LREE exchange probably took place as well. Domanik et al. (2005) mention finding fluorapatite in Johnstown, LAP 02216 and Shalka, but do not describe the textural setting. These authors discuss Ca-phosphates (fluorapatite and whitlockite) in Manegaon and Roda, where they are usually associated with diopside and/or metal + troilite, and sometimes with a silica phase. Domanik et al. (2005) observed that Manegoan and Roda have greater abundances of phosphates than found in most diogenites.

One condition that must be met in order for the diffusion mechanism to work is that $D^{phos/opx}{}_{Eu^{2+}}$ must increase with falling temperature. This will favor transport of Eu^{2+} out of orthopyroxene into the phosphate. We know of no experimental study of the

effects of temperature on $D^{phos/opx}$; however, it is plausible that this partition coefficient would have increased with falling temperature in diogenite plutons. Orthopyroxene/melt REE partition coefficients are directly correlated with D_{Ca} (e.g., Jones 1995). This is understandable because the larger Ca^{2+} ion distorts the pyroxene M2 site, making it more favorable for incorporation of the REE. At lower temperature, orthopyroxene can contain less Ca than at higher temperature (cf. the two-pyroxene thermometer of Lindsley and Anderson 1983), implying that Eu^{2+} would also be excluded at lower *T*. By contrast, Ca-phosphates are favorable hosts for REE. Merrilite (whitlockite)/melt partition coefficients are >1 for REE and Sr (Dickinson and Hess 1983). Calcium phosphates in diogenites have very high concentrations of REE, at weight percent concentrations for the LREE (Mittlefehldt 1994; Domanik et al. 2004, 2005). It is thus very likely that with decreasing *T*, $D^{phos/opx}$ for Eu^{2+} will increase.

Figure 6 shows our analyses of GRA 98108 along with the leached diogenites of Barrat et al. (2010). Our samples were untreated by mineral acids and any phosphates they may have contained were included in the analyzed samples. The GRA 98108 sample analyzed by ICP-MS has a very low Eu/Eu*, and plots very near the orthopyroxene cumulate line using the Sr (Eu^{2+} analog) partition coefficient. GRA 98108 contains olivine—18.5 vol% in the thin section studied by Beck and McSween (2010)—but this will not greatly affect the ratio of Eu to Gd in the cumulate because of the very low partition coefficients for olivine (cf. McKay 1986). GRA 98108 is plagioclase-bearing, but Beck and McSween (2010) measured only 0.3 vol% in their thin section. The bulk samples we have analyzed are low in plagioclase as indicated by the low Na and Al contents (Tables 6–8; Fig. 3). However, GRA 98108 is heterogeneous in its olivine and orthopyroxene distribution (see fig. 1 of Righter 2001), and plagioclase may be heterogeneously distributed on the centimeter-scale. In the thin section we studied (,15), plagioclase is not uniformly distributed, but rather is concentrated along the margin between an olivine-rich region and an orthopyroxene-rich region. Thus, either under- or oversampling of plagioclase relative to that of a true "bulk rock" sample could easily occur. Our INAA sample has higher Na and Eu contents than the ICP-MS samples (Tables 7 and 8) indicating a greater plagioclase content in the former. The INAA sample plots in the region of cumulate plus trapped melt on Fig. 6. (For the INAA sample, the Gd concentration was calculated by interpolation of the REE pattern.) Our GRA 98108 data do not prove that subsolidus diffusion of Eu^{2+} from orthopyroxene to plagioclase coupled with undersampling plagioclase engendered the very low Eu/Gd ratio of the ICP-MS sample, but they are consistent with this hypothesis.

A counter argument to our hypothesis is provided by Dhofar 700. The leached residues of this diogenite have Eu/Eu* of 0.09–0.13 (Barrat et al. 2010). The two samples with the lowest LREE contents plot below the Eu/Eu*-Gd/Lu trend of diogenites in Fig. 7a, but within the field of low Eu/Eu*, La/Sm diogenites in Fig. 7b. (We ignore the LREE-rich samples of this Omani meteorite because of the possibility of terrestrial contamination of the LREE (cf. Barrat et al. 2003), which may not be removed by HCl.) Yamaguchi et al. (2011) have argued that several diogenites, including Dhofar 700, were cooled quickly, nearer the vestan surface than most diogenites because their pyroxenes have Fe-Mg zoning near grain rims. These authors calculate a diffusion profile between olivine in an inclusion and the host orthopyroxene and match it with a cooling rate of 1000° per annum. This would preclude generation of the very low Eu/Eu* for Dhofar 700 pyroxenes by the mechanism we postulate. However, Dhofar 700 is somewhat unusual for a diogenite. It has higher Sc and Mn contents than other diogenites, and a lower Fe/Mn, suggesting that its origin may not be typical of diogenites. Detailed petrologic study and in situ trace element analyses of this diogenite should be done to determine its origin.

Barrat et al. (2010) considered the low Eu/Eu* of their leaching residues to be innate to the orthopyroxene cumulate and thus can be used to infer magma compositions. Following Treiman (1996), we consider that the low Eu/Eu* of the leaching residues more likely represents orthopyroxene that equilibrated with Ca phosphate (and/or plagioclase) at low, subsolidus temperatures. In particular, our hypothesis is that because of the more rapid diffusion of Eu^{2+} relative to Eu^{3+} (Cherniak and Liang 2007), the Eu/Eu* of orthopyroxene was lowered by this mechanism. A corollary is that the leaching residues cannot be used as a guide to diogenite parent magma compositions. Because of the heterogeneous distribution of minor phases in many diogenites, even analyses of bulk rock samples must be interpreted cautiously.

Diogenite Formation—An Unresolved Problem

If the Barrat et al. (2010) hypothesis is rejected, how then were diogenites formed? Mittlefehldt (1994) and Fowler et al. (1995) discussed the problems with modeling diogenites as cumulates from a vestan magma ocean; incompatible lithophile elements suggest extensive igneous fractionation within the diogenite suite, yet plagioclase and calcic pyroxene that would be expected to appear on the liquidus, are typically minor or accessory phases, or are absent (Bowman et al. 1997; Beck and McSween 2010). This led to the suggestion that

diogenites may have formed from parent melts that are either highly orthopyroxene-normative, or basaltic but with variable initial incompatible element contents (Mittlefehldt 1994; Fowler et al. 1995). Either scenario suggests a partial melting origin for diogenite parent melts, not as an intermediate magma formed from a global magma system.

Mittlefehldt (2000) presented evidence that EETA79002 contains impact-mixed material from at least three diogenitic plutons; a magnesian harzburgitic body, an orthopyroxenite like typical diogenites, and one or two ferroan orthopyroxenites. Eucritic debris was not found, and plagioclase is rare in EETA79002. Bowman et al. (1997) reported 0.3 vol% plagioclase in one thin section, but none in two others. Thus, EETA79002 is an impact-produced mixture of several ultramafic plutons without basaltic contamination. Mittlefehldt (2000) suggested that this is most compatible with formation of the EETA79002 protoliths within the vestan crust, not as a deep-seated layer below a basaltic crust because otherwise, eucritic debris ought to be present. Mittlefehldt (2000) concluded that the different lithologic components were formed in kilometer-scale intrusions that were mixed by small-scale impacts.

Shearer et al. (1997, 2010) championed the multiple-basaltic-parent-melt hypothesis, and concluded that diogenites were formed in many different layered intrusions. This model too has its problems, chiefly that the origin of the wide range in trace element contents of diogenites is not explained; it is merely pushed back to an earlier stage of the petrogenetic process and left unaddressed.

Despite these problems, our opinion is that models such as those advocated by Shearer et al. (2010) are more plausible mechanisms for diogenite petrogenesis. Nevertheless, the petrogenesis of diogenites remains an unsolved part of the overall petrologic evolution of 4 Vesta.

CONCLUSIONS

Two brecciated diogenites, ALH 85015 and PCA 02008, have higher contents of the major elements Al_2O_3 and CaO compared to most diogenites, and have higher incompatible trace lithophile element concentrations than typically observed for diogenites. These breccias also contain small amounts of basaltic (eucritic) debris. Mafic debris is also present in PCA 02017, a suggested pair of PCA 02008. Pyroxene compositions in mafic clasts in PCA 02017 have compositions similar to those of cumulate eucrites and basaltic eucrites, but some are more ferroan (mg# $\sim$28) than found in eucrites. These diogenites are polymict breccias, and the unusual compositional characteristics of them are due to contamination by mafic lithologies.

QUE 93009 is an unusual diogenite that has pyroxene compositions at the ferroan end of the diogenite range, contains coarse-grained norititc clasts, and has chromite grains with ilmenite exsolution lamellae. No basaltic material has been observed in this breccia. QUE 93009 has higher concentrations of incompatible lithophile elements than do most other nonpolymict diogenites. It shares some petrologic and compositional characteristics with the Yamato Type B diogenites, although there are distinctions as well. QUE 93009 is possibly a transitional rock type between classic, magnesian diogenites and magnesian cumulate eucrites, such as the cumulate component of the Binda polymict cumulate eucrite.

LEW 88679 has anomalously low concentrations of the most highly incompatible elements (Nb, LREE, Ta, Th, U) relative to elements that are not as highly incompatible (Y, Zr, Yb, Lu, Hf) when compared to most diogenites. LEW 88679 is a dimict breccia composed of more magnesian harzburgite and more ferroan orthopyroxenite (Beck and McSween 2010). It is unlikely that its low incompatible element contents are caused by the absence of a trapped melt component because it is unlikely that the two lithologic units in LEW 88679 would both be atypically poor in trapped melt compared to most diogenites. A plausible explanation is that mobilization of the incompatible lithophile elements occurred after assembly of the breccia on Vesta, but the nature and details of the process are not known. This was not the thermal metamorphic event that decoupled Fe-Mg from incompatible trace elements in diogenites generally.

The very low Eu/Eu* ratios of diogenite orthopyroxenes (acid-washed bulk samples) have been cited as evidence that mixing of diogenite parent magmas with low-degree melts of the basaltic crust occurred (Barrat et al. 2010). We find that this interpretation is not compelling. Subsolidus equilibration has mobilized major elements in orthopyroxenes resulting in Fe-Mg exchange (Mittlefehldt 1994). This process may have caused exchange of Eu^{2+} over greater distances than for Sm, Eu^{3+}, or Gd because of the higher diffusion coefficient of the former (Cherniak and Liang 2007). Exchange of Eu^{2+} between REE-poor orthopyroxene and REE-rich phosphate during equilibration on the parent asteroid, followed by laboratory dissolution of phosphates prior to analysis, would result in a residue with an Eu/Eu* much lower than that of the original cumulate. Remembering past cautions (Treiman 1996), we suggest that leached diogenite samples cannot be used to infer parent magma compositions or constrain the processes by which they were formed.

We favor an origin for diogenites as cumulates from multiple-layered basic intrusions in the vestan crust (e.g., Shearer et al. 2010). Nevertheless, this model leaves some key observations on diogenites poorly explained. For

example, the absence of mafic lithologies (plagioclase + clinopyroxene) in the breccias is difficult to understand, especially for those diogenites that are composed of two or more ultramafic lithologies. This problem also applies to the Barrat et al. (2010) scenario. The multiple intrusion model does not seem to be consistent with the consensus model for eucrite genesis in a global magma ocean. A compelling petrogenesis model for the diogenites has yet to emerge.

Acknowledgments—We thank the National Science Foundation for funding the ANSMET collecting teams that brought back the Antarctic samples studied here, and the Meteorite Working Group, NASA JSC, and the National Museum of Natural History (Smithsonian Institution) for allocation of the samples. We thank K. J. Domanik and the late M. J. Drake of the University of Arizona for providing the sample of Bilanga studied here. This work was funded through the NASA Cosmochemistry Program to D. W. M. and Cosmochemistry grant NNG06GG36G to H. Y. M. We thank MAPS AE R. Korotev and referees J.-A. Barrat and "anonymous" for thorough reviews and editorial handling that greatly improved the quality of this article.

Editorial Handling—Dr. Randy Korotev

REFERENCES

Barrat J. A. 2004. Determination of parental magmas of HED cumulates: The effects of interstitial melts. *Meteoritics & Planetary Science* 39:1767–1779.

Barrat J. A., Gillet P., Lesourd M., Blichert-Toft J., and Poupeau G. R. 1999. The Tatahouine diogenite: Mineralogical and chemical effects of sixty-three years of terrestrial residence. *Meteoritics & Planetary Science* 34:91–97.

Barrat J. A., Jambon A., Bohn M., Blichert-Toft J., Sautter V., Göpel C., Gillet P., Boudouma O., and Keller F. 2003. Petrology and geochemistry of the unbrecciated achondrite Northwest Africa 1240 (NWA 1240): An HED parent body impact melt. *Geochimica et Cosmochimica Acta* 67:3959–3970.

Barrat J. A., Yamaguchi A., Greenwood R. C., Bohn M., Cotten J., Benoit M., and Franchi I. A. 2007. The Stannern trend eucrites: Contamination of main group eucritic magmas by crustal partial melts. *Geochimica et Cosmochimica Acta* 71:4108–4124.

Barrat J. A., Yamaguchi A., Benoit M., Cotten J., and Bohn M. 2008. Geochemistry of diogenites: Still more diversity in their parental melts. *Meteoritics & Planetary Science* 43:1759–1775.

Barrat J.-A., Yamaguchi A., Zanda B., Bollinger C., and Bohn M. 2010. Relative chronology of crust formation on asteroid Vesta: Insights from the geochemistry of diogenites. *Geochimica et Cosmochimica Acta* 74:6218–6231.

Beattie P. 1993. The generation of uranium series disequilibria by partial melting of spinel peridotite; constraints from partitioning studies. *Earth and Planetary Science Letters* 117:379–391.

Beck A. W. and McSween H. Y. 2010. Diogenites as polymict breccias composed of orthopyroxenite and harzburgite. *Meteoritics & Planetary Science* 45:850–872, doi:10.1111/j.1945-5100.2010.01061.x.

Beck A. W., McSween H. Y., Mittlefehldt D. W., and Lee C.-T. A. 2008. Fused bead analysis in diogenite meteorites (abstract #1177). 40th Lunar and Planetary Science Conference. CD-ROM.

Beck A. W., Mittlefehldt D. W., McSween H. Y. Jr., Rumble D. III, Lee C.-T. A., and Bodnar R. J. 2011. MIL 03443, a dunite from asteroid 4 Vesta: Evidence for its classification and cumulate origin. *Meteoritics & Planetary Science* 46:1133–1151.

Beck A. W., McSween H. Y. Jr., and Bodnar R. J. Forthcoming. In situ laser ablation ICP-MS determination of trace element concentrations in dimict diogenite: Further evidence for harzburgitic and orthopyroxenitic lithologies. *Meteoritics & Planetary Science*.

Bédard J. H. 2007. Trace element partitioning coefficients between silicate melts and orthopyroxene: Parameterizations of D variations. *Chemical Geology* 244:263–303.

Berkley J. L. and Boynton N. J. 1992. Minor/major element variation within and among diogenite and howardite orthopyroxenite groups. *Meteoritics* 27:387–394.

Binzel R. P. and Xu S. 1993. Chips off asteroid 4 Vesta: Evidence for the parent body of basaltic achondrite meteorites. *Science* 260:186–191.

Bowman L. E., Spilde M. N., and Papike J. J. 1997. Automated energy dispersive spectrometer modal analysis applied to the diogenites. *Meteoritics & Planetary Science* 32:869–875.

Bowman L. E., Papike J. J., and Spilde M. N. 1999. Diogenites as asteroidal cumulates: Insights from spinel chemistry. *American Mineralogist* 84:1020–1026.

Brown R. W. 1977. A sample fusion technique for whole rock analysis with the electron microprobe. *Geochimica et Cosmochimica Acta* 41:435–438.

Bunch T. E., Irving A. J., Wittke J. H., Kuehner S. M., and Rumble D. III. 2007. Distinctive magnesian, protogranular and polymict diogenites from Northwest Africa, Oman and United Arab Emirates (abstract). *Meteoritics & Planetary Science* 42:A27.

Cherniak D. J. and Liang Y. 2007. Rare earth element diffusion in natural enstatite. *Geochimica et Cosmochimica Acta* 71:1324–1340.

Consolmagno G. J. 1979. REE patterns versus the origin of the basaltic achondrites. *Icarus* 40:522–530.

Consolmagno G. J. and Drake M. J. 1977. Composition and evolution of the eucrite parent body: Evidence from rare earth elements. *Geochimica et Cosmochimica Acta* 41:1271–1282.

Delaney J. S., Takeda H., Prinz M., Nehru C. E., and Harlow G. E. 1983. The nomenclature of polymict basaltic achondrites. *Meteoritics* 18:103–111.

Delaney J. S., Prinz M., and Takeda H. 1984. The polymict eucrites. *Journal of Geophysical Research Supplement* 89:C251–C288.

Dickinson J. E. and Hess P. C. 1983. Role of whitlockite and apatite in lunar felsites (abstract). 14th Lunar and Planetary Science Conference. pp. 158–159.

Domanik K., Kolar S., Musselwhite D., and Drake M. J. 2004. Accessory silicate mineral assemblages in the Bilanga diogenite: A petrographic study. *Meteoritics & Planetary Science* 39:567–579.

Domanik K. J., Sideras L. C., and Drake M. J. 2005. Olivine and Ca-phosphate in the diogenites Manegaon and Roda (abstract #2128). 36th Lunar and Planetary Science Conference. CD-ROM.

Drake M. J. 1979. Geochemical evolution of the eucrite parent body: Possible nature and evolution of asteroid 4 Vesta. In *Asteroids*, edited by Gehrels T. Tucson, Arizona: The University of Arizona Press. pp. 765–782.

Drake M. J. and Weill D. F. 1975. Partition of Sr, Ba, Ca, Y, Eu^{2+}, Eu^{3+}, and other REE between plagioclase feldspar and magmatic liquid: An experimental study. *Geochimica et Cosmochimica Acta* 39:689–712.

Duke M. B. and Silver L. T. 1967. Petrology of eucrites, howardites and mesosiderites. *Geochimica et Cosmochimica Acta* 31:1637–1665.

Eggins S. M., Woodhead J. D., Kinsley L. P. J., Mortimer G. E., Sylvester P., McCulloch M. T., Hergt J. M., and Handler M. R. 1997. A simple method for the precise determinations of ≥40 trace elements in geological samples by ICPMS using enriched isotope internal standardisation. *Chemical Geology* 134:311–326.

Fowler G. W., Papike J. J., Spilde M. N., and Shearer C. K. 1994. Diogenites as asteroidal cumulates: Insights from orthopyroxene major and minor element chemistry. *Geochimica et Cosmochimica Acta* 58:3921–3929.

Fowler G. W., Shearer C. K., Papike J. J., and Layne G. D. 1995. Diogenites as asteroidal cumulates: Insights from orthopyroxene trace element chemistry. *Geochimica et Cosmochimica Acta* 59:3071–3084.

Fukuoka T., Boynton W. V., Ma M.-S., and Schmitt R. A. 1977. Genesis of howardites, diogenites, and eucrites. Proceedings, 8th Lunar Science Conference. pp. 187–210.

Gooley R. C. 1972. Chemistry and mineralogy of the diogenites. Ph.D. dissertation, Arizona State University, Tempe, Arizona, USA.

Greenwood R. C., Franchi I. A., Jambon A., and Buchanan P. C. 2005. Widespread magma oceans on asteroidal bodies in the early solar system. *Nature* 435:916–918.

Jones J. H. 1995. Experimental trace element partitioning. In *Rock physics and phase relations. A handbook of physical constants*, AGU Reference Shelf 3, edited by Ahrens T. J. Washington, D.C.: The American Geophysical Union. pp. 73–104.

Keil K. 2002. Geological history of asteroid 4 Vesta: The "smallest terrestrial planet." In *Asteroids III*, edited by Bottke W., Cellino A., Paolicchoi P., and Binzel R. P. Tucson, Arizona: The University of Arizona Press. pp. 573–584.

Lambert D. D. and Simmons E. C. 1987. Magma evolution in the Stillwater complex, Montana: I. Rare-earth element evidence for the formation of the ultramafic series. *American Journal of Science* 287:1–32.

Lee C.-T. A., Oka M., Luffi P., and Agranier A. 2008. Internal distribution of Li and B in serpentinites from the Feather River Ophiolite, California, based on laser ablation inductively coupled plasma mass spectrometry. *Geochemistry Geophysics Geosystems* 9:Q12011, doi:10.1029/2008GC002078.

Lindsley D. H. and Anderson D. J. 1983. A two-pyroxene thermometer. *Journal of Geophysical Research Supplement* 88:A887–A906.

Lindstrom D. J. and Korotev R. L. 1982. TEABAGS: Computer programs for instrumental neutron activation analysis. *Journal of Radioanalytical Chemistry* 70:439–458.

Mason B., Jarosewich E., and Nelen J. A. 1979. The pyroxene-plagioclase achondrites. *Smithsonian Contributions to the Earth Sciences* 22:27–45.

McCord T. B., Adams J. B., and Johnson T. V. 1970. Asteroid Vesta: Spectral reflectivity and compositional implications. *Science* 168:1445–1447.

McKay G. A. 1986. Crystal/liquid partitioning of REE in basaltic systems: Extreme fractionation of REE in olivine. *Geochimica et Cosmochimica Acta* 50:69–79.

McKay G., Wagstaff J., and Le L. 1990. REE distribution coefficients for pigeonite: Constraints on the origin of the mare basalt europium anomaly (abstract). 21st Lunar and Planetary Science Conference. pp. 773–774.

McSween H. Y., Mittlefehldt D. W., Beck A., Mayne R., and McCoy T. J. 2011. HED meteorites and their relationship to the geology of Vesta and the Dawn mission. *Space Science Reviews*, doi:10.1007/s11214-010-9637-z.

Mittlefehldt D. W. 1979. Petrographic and chemical characterization of igneous lithic clasts from mesosiderites and howardites and comparison with eucrites and diogenites. *Geochimica et Cosmochimica Acta* 43:1917–1935.

Mittlefehldt D. W. 1994. The genesis of diogenites and HED parent body petrogenesis. *Geochimica et Cosmochimica Acta* 58:1537–1552.

Mittlefehldt D. W. 2000. Petrology and geochemistry of the Elephant Moraine A79002 diogenite; A genomict breccia containing a magnesian harzburgite component. *Meteoritics & Planetary Science* 35:901–912.

Mittlefehldt D. W. 2002. Geochemistry of new, unusual diogenites and constraints on diogenite genesis (abstract). *Meteoritics & Planetary Science* 37:A100.

Mittlefehldt D. W. and Lindstrom M. M. 1991. Generation of abnormal trace element abundances in Antarctic eucrites by weathering processes. *Geochimica et Cosmochimica Acta* 55:77–87.

Mittlefehldt D. W. and Lindstrom M. M. 1993. Geochemistry and petrology of a suite of ten Yamato HED meteorites. *Antarctic Meteorite Research* 6:268–292.

Mittlefehldt D. W. and Lindstrom M. M. 2001. Petrology and geochemistry of Patuxent Range 91501, an impact melt from the L-chondrite parent body, and Lewis Cliff 88663, an L7 chondrite. *Meteoritics & Planetary Science* 36:439–457.

Mittlefehldt D. W. and Lindstrom M. M. 2003. Geochemistry of eucrites: Genesis of basaltic eucrites, and Hf and Ta as petrogenetic indicators for altered Antarctic eucrites. *Geochimica et Cosmochimica Acta* 67:1911–1935.

Mittlefehldt D. W., McCoy T. J., Goodrich C. A., and Kracher A. 1998. Non-chondritic meteorites from asteroidal bodies. In *Planetary materials*, edited by Papike J. J. Reviews in Mineralogy, vol. 36. Washington, D.C.: Mineraological Society of America. pp. 4-1–4-195.

Mittlefehldt D. W., Beck A. W., Lee C.-T. A., and McSween H. Y. Jr 2009. Chemistry of diogenites and evolution of their parent asteroid (abstract #1038). 40th Lunar and Planetary Science Conference. CD-ROM.

Norman M., Garcia M. O., and Pietruszka A. J. 2005. Trace-element distribution coefficients for pyroxenes, plagioclase, and olivine in evolved tholeiites from the 1955 eruption of Kilauea Volcano, Hawaii, and petrogenesis of differentiated rift-zone lavas. *American Mineralogist* 90: 888–899.

Papike J. J., Shearer C. K., Spilde M. N., and Karner J. M. 2000. Metamorphic diogenite Grosvenor Mountains 95555:

Mineral chemistry of orthopyroxene and spinel and comparisons to the diogenite suite. *Meteoritics & Planetary Science* 35:875–879.
Righter K. 2001. Petrography, mineralogy and petrology of two new HED meteorites: Diogenite GRA 98108 and howardite GRA 98030 (abstract #1765). 32nd Lunar and Planetary Science Conference. CD-ROM.
Righter K. and Drake M. J. 1997. A magma ocean on Vesta: Core formation and petrogenesis of eucrites and diogenites. *Meteoritics & Planetary Science* 32:929–944.
Righter K. and Shearer C. K. 2003. Magmatic fractionation of Hf and W: Constraints on the timing of core formation and differentiation in the Moon and Mars. *Geochimica et Cosmochimica Acta* 67:2497–2507.
Ruzicka A., Snyder G. A., and Taylor L. A. 1997. Vesta as the howardite, eucrite and diogenite parent body: Implications for the size of a core and for large-scale differentiation. *Meteoritics & Planetary Science* 32:825–840.
Sack R. O., Azeredo W. J., and Lipschutz M. E. 1991. Olivine diogenites: The mantle of the eucrite parent body. *Geochimica et Cosmochimica Acta* 55:1111–1120.
Schwandt C. S. and McKay G. A. 1998. Rare earth element partition coefficients from enstatite/melt synthesis experiments. *Geochimica et Cosmochimica Acta* 62:2845–2848.
Shearer C. K., Fowler G. W., and Papike J. J. 1997. Petrogenetic models for magmatism on the eucrite parent body: Evidence from orthopyroxene in diogenites. *Meteoritics & Planetary Science* 32:877–889.
Shearer C. K., Burger P., and Papike J. J. 2010. Petrogenetic relationships between diogenites and olivine diogenites: Implications for magmatism on the HED parent body. *Geochimica et Cosmochimica Acta* 74:4865–4880.
Stolper E. 1977. Experimental petrology of eucrite meteorites. *Geochimica et Cosmochimica Acta* 41:587–611.
Takeda H. and Mori H. 1985. The diogenite-eucrite links and the crystallization history of a crust of their parent body. *Journal of Geophysical Research Supplement* 90:C636–C648.
Takeda H., Miyamoto M., Ishii T., and Reid A. M. 1976. Characterization of crust formation on a parent body of achondrites and the Moon by pyroxene crystallography and chemistry. Proceedings, 7th Lunar Science Conference. pp. 3535–3548.
Treiman A. H. 1996. The perils of partition: Difficulties in retrieving magma compositions from chemically equilibrated basaltic meteorites. *Geochimica et Cosmochimica Acta* 60: 147–155.
Warren P. H. 1985. Origin of howardites, diogenites and eucrites: A mass balance constraint. *Geochimica et Cosmochimica Acta* 49:577–586.
Warren P. H. 1997. Magnesium oxide-iron oxide mass balance constraints and a more detailed model for the relationship between eucrites and diogenites. *Meteoritics & Planetary Science* 32:945–963.
Warren P. H., Kallemeyn G. W., Huber H., Ulff-Møller F., and Choe W. 2009. Siderophile and other geochemical constraints on mixing relationships among HED-meteoritic breccias. *Geochimica et Cosmochimica Acta* 73:5918–5943.
Welten K. C., Caffee M. W., and Beck A. W. 2009. Cosmogenic radionuclides in three paired howardites and a polymict diogenite from Pecora Escarpment icefield, Antarctica (abstract). *Meteoritics & Planetary Science* 44:A216.
Yamaguchi A., Barrat J.-A., Ito M., and Bohn M. 2011. Posteucritic magmatism on Vesta: Evidence from the petrology and thermal history of diogenites. *Journal of Geophysical Research Planets* 116:E08009, doi:10.1029/2010JE003753.

SUPPORTING INFORMATION

Additional supporting information may be found in the online version of this article:

Tables S1 through S5. Analytical details on the INAA and ICP-MS determinations on individual diogenites and international reference materials analyzed as controls.

Please note: Wiley-Blackwell is not responsible for the content or functionality of any supporting materials supplied by the authors. Any queries (other than missing material) should be directed to the corresponding author for the article.